# Photophysics of Methylammonium Lead Tribromide Perovskite: Free Carriers, Excitons and Sub-Bandgap States

*Nikolaos Droseros, Demetra Tsokkou, Natalie Banerji**

Department of Chemistry and Biochemistry, University of Bern, Freiestrasse 3, CH-3012 Bern, Switzerland

Corresponding Author: Dr. Natalie Banerji
Department of Chemistry and Biochemistry, University of Bern, Freiestrasse 3, CH-3012 Bern, Switzerland
E-mail: natalie.banerji@dcb.unibe.ch

Keywords: (($MAPbBr_3$, photoluminescence, disorder, traps, dynamics))

## Abstract

Methylammonium lead tribromide perovskite, one of the first artificially synthesized perovskites, can be used in multijunction solar cells and for light emitting applications. Its structure leads to a wide direct bandgap, to a high extinction coefficient for absorption and to an exciton binding energy that is higher than the thermal energy at room temperature. The broad range of studies performed on the optical phenomena in this material has revealed the contribution of free carriers, excitons and defect states to the photoluminescence properties. The present report aims to highlight the role played by the different primary photoexcitations, by defects and by a variety of optical phenomena (dual emission, re-absorption, photon-recycling, Rashba-splitting) on the observed excited-state properties of this semiconductor. Focus is given to the manifestation of these properties in different spectroscopic measurements.

## 1. Introduction

Methylammonium lead tribromide perovskite ($MAPbBr_3$) is one of the first artificially synthesized perovskites.[1],[2],[3],[4],[5] Although it has a higher stability (even without specific treatments),[6],[7],[8] and a higher photovoltage compared to the iodide equivalent, methylammonium lead triiodide ($MAPbI_3$),[9] its high binding energy with respect to thermal energy at room temperature (RT) makes $MAPbBr_3$ less suitable for applications in single junction solar cells (SCs), with a maximum achieved photon conversion efficiency (PCE) of only 10.4%.[10] Nevertheless, it is a possible candidate as photoactive layer in multijunction SCs.[11] Most importantly, its convenient thin-film processing from solution and strong green

emission allow light emitting applications.[12],[13],[14],[15],[16],[17],[18],[19],[20] In an early study, Cho et al. have shown that it is possible to achieve high efficiency in $MAPbBr_3$ light emitting diodes (LEDs), by preventing the formation of metallic lead (Pb) atoms that cause exciton quenching and by spatially confining the excitons, thus demonstrating at the same time that excitons play an important role in the emission from this material.[21] Since then, many studies have focused on improving the emission properties of $MAPbBr_3$ by using different techniques in order to passivate traps on the surface, while an increased exciton confinement has been realized by reducing the dimensionality of the material.[22],[23],[24],[25],[26],[27]

Besides the achievement of high photoluminescence (PL) quantum yield (QY) in $MAPbBr_3$, its emission properties are very intriguing and will be a main focus of the current Progress Report. The attribution of the PL spectral shape and peak position has proven to be non-trivial, since many phenomena affect the emission. The high extinction coefficient and the small Stokes shift between the absorption and the emitted PL gives rise to strong re-absorption effects, while the presence of both free carriers and excitons makes the PL emission strongly excitation density dependent.[28],[29],[30] Similarly to other perovskites, $MAPbBr_3$ undergoes phase transitions at 80 K (orthorhombic II to orthorhombic I), at 145 K (orthorhombic I to tetragonal) and at 210 K (tetragonal to cubic),[31] thus further complicating temperature-dependent optical measurements and contributing to the uncertainty of the binding energies measured at different temperatures.[3],[32],[33] In addition, photon recycling has been suggested to facilitate the radiative transport of the photoexcited species and to increase the quasi-Fermi level splitting, as will be examined further below.[34], [35], [36],[37], [38] Moreover, the PL properties on the surface of large $MAPbBr_3$ single crystals have been found to be different than in the bulk. In this context, a different bandgap or a different phase at the surface with respect to the bulk has been proposed. Also, the coexistence of ordered and disordered $MAPbBr_3$ domains has been suggested. Finally, the presence of both spin-orbit coupling (SOC) and symmetry breaking in this material results in a strong Rashba-like spin-split that can contribute to the PL emission.

Apart from these phenomena, the excited-state species in $MAPbBr_3$ are strongly influenced by intrinsic disorder that manifests itself in the form of tail states in the sub-bandgap absorption (Urbach tail), and by defects that occupy states either close to the band edge or deeper in the bandgap. The role of disorder, defects and traps will be the second topic covered in this report. Although not many types of defects are stable in the perovskite structure, the excited-state dynamics can still be influenced by traps that are formed during film deposition. It will be discussed how defects can either improve or deteriorate the PL emission, while they contribute to the excitation density-dependent dynamics of the photoexcited species at long times. Besides

lead (Pb), bromide (Br) and methylammonium (MA), also methylamine ($MA^*$), which is present upon film deposition of $MAPbBr_3$, has been reported to cause defect formation similar as has been shown in $MAPbI_3$. In addition, the effect of the cation on the formation of different defects and on ion migration has been studied and will be reviewed.[39],[40]

Finally, the present report aims to discuss how the effect of different primary photoexcitations, of defects and of a variety of optical phenomena (re-absorption, photon-recycling, Rashba-splitting) manifest in different spectroscopic measurements, including not only PL but also ultrafast transient absorption (TA) techniques. This allows, in particular, to investigate how excitons are formed and their subsequent fate (recombination or dissociation), which are important factors for LED device performance.

## 2. Photoluminescence properties

### 2.1. Origin of the PL emission: Excitons versus free carriers

A characteristic of perovskites is the presence of PL emission even at RT that ultimately results in high conversion efficiencies in SCs[4],[41],[42],[43] and LEDs.[21],[44],[45] Compared to other inorganic semiconductors, where the RT emission originates from trap and defect states, band-to-band PL emission is often observed in halide perovskites, a strong indication of small trap densities. Richter et al. have confirmed experimentally that the emission from $MAPbBr_3$ originates from a direct bandgap transition,[46] by showing that the PL takes place from cold carriers that have relaxed to the band edge. In this section, the origin of the band-to-band emission in $MAPbBr_3$ is discussed in terms of excitons and free charges.

The fundamental species generated upon photoexcitation (either free charges, excitons or a mixture of both) is largely dependent on the exciton binding energy $E_b$. For instance in $MAPbI_3$ - the most studied perovskite - low values of $E_b$ (2-25 meV),[47],[48],[49],[32],[50],[51],[52],[53] close to or smaller than the thermal energy at RT ($k_BT$ = 25 meV), lead to primarily free charges in the excited state, which is beneficial for SC applications.[51],[54],[55],[56],[57],[58] Hence, this quantity is crucial for determining the mode of operation of $MAPbBr_3$ in optoelectronic devices and has been extensively investigated. Table 1 shows the values of $E_b$ reported in various publications for three-dimensional (3D) $MAPbBr_3$.[59] These values have been estimated using a variety of methods such as temperature- and excitation density- dependent PL,[28],[29],[33],[60],[61] PL reflectance,[60],[62] electroluminescence and electroabsorption,[63] magneto-absorption/transmittance,[3],[32] optical absorption,[50],[52],[63],[64],[65],[66],[67],[68] permittivity measurements,[69] and theoretical calculations.[70],[71] It is interesting to note that different

techniques yield different values of $E_b$ even for the same sample. For example, Rana et al.[63] have reported a different $E_b$ for the absorbing and the emitting exciton when studying the same NCs with two different techniques. However, independently of the observed differences, all studies evidence a higher $E_b$ in $MAPbBr_3$ compared to its iodide counterpart, showing that the halogen substitution results in more bound excitons. The values of $E_b$ range between 15.3-150 meV depending on the technique and the on type of sample (polycrystalline or single crystal). Indeed, the crystal size, crystal quality, chemical environment, dielectric constant of the surroundings and perovskite dimensionality can all strongly affect $E_b$, which can increase it up to 375 meV for small nanocrystals (NCs), as seen in Table 1.[29],[32],[52],[69],[70], [61] An $E_b$ of hundreds of meVs far exceeds the thermal energy at RT, ensuring the generation of excitons as predominant species upon photoexcitation and moreover preventing their dissociation prior to radiative decay.

**Table 1.** $E_b$ of $MAPbBr_3$ films, single crystals and NCs reported in different publications. The method used in each case to find $E_b$ is mentioned.

| Publication | Technique | Sample | Value |
|---|---|---|---|
| Zheng et al. [29] | Temperature-dependent PL | Microcrystalline polygonal disks with thickness of 1.6 μm and 15 μm diameter | 84 meV |
| Zheng et al. [29] | Temperature-dependent PL | NCs (8.2 nm) | 320 meV |
| Tanaka et al.[3] | Magneto-absorption at 4.2 K | Polycrystalline thin film | 76 meV |
| Yang et al. [66] | UV−vis absorption spectra (Elliot formula) | Polycrystalline thin film (86 nm) | 40 meV |
| Koutselas et al.[70] | Variational calculations | - | 150 meV |
| Galkowski et al.[32] | Magneto-absorption at 2 K | Polycrystalline thin film | 25 meV |
| Sestu et al.[52] | UV−vis absorption (absorption F-sum rule on integrated absorption) | Thin film | 60 meV |
| Comin et al.[64] | UV−vis absorption | Polycrystalline thin film | 21 meV |
| Shi. et al. [65] | UV−vis absorption | Single crystal | 75 meV |
| Soufiani et al.[69] | Permittivity measurements | Polycrystalline thin film | 35 meV |
| Ruf et al. [50] | UV−vis absorption spectra (Elliot formula) | Polycrystalline thin film (350-450nm) | 36 meV at 10 K, 41 meV at RT |
| Rana et al.[63] | UV−vis absorption spectra (Elliot formula) and temperature-dependent electroabsorption | Polycrystalline thin film | 17 meV |
| Rana et al.[63] | UV−vis absorption spectra (Elliot formula) and temperature-dependent electroabsorption | NCs (6 nm) | 17 meV |

| | | | |
|---|---|---|---|
| Rana et al.[63] | Temperature-dependent PL | NCs (6 nm) | 70 meV |
| Liu et al.[33] | Temperature dependent PL | Thin film with crystallites of 100s nm to a few μm size | 25.9 meV |
| Droseros et al.[28] | Excitation density-dependent integrated PL | Polycrystalline thin film | 110 meV |
| Kunugita et al.[60] | Temperature-dependent PL and reflectance | Single crystal | 80-100 meV |
| Tilchin et al.[72] | Temperature-dependent PL and reflectance | Single crystal | 15.33 meV |
| Do et al.[62] | Temperature dependent PL and reflectance | Single crystal | 21 meV (low energy exciton), 90 meV (high energy exciton) |
| Saba et al. [67] | UV−vis absorption spectra (Elliot formula).* | Polycrystalline thin film | 64 meV |
| Zhang et al. [61] | Temperature-dependent PL | micrometer-sized particle | 65 meV |
| Zhang et al. [61] | Temperature-dependent PL | NCs (3.3 nm) | 375 meV |
| Hu et al. [68] | UV−vis absorption | Polycrystalline thin film | 80 meV |
| Bokdam et al.[71] | Density functional theory (DFT) calculations | - | 71 meV |

*Notes:* The experimental spectra were taken by ref.* [64] *and then fitted by the authors of ref.* [67]

While a high $E_b$ hampers the charge separation in SCs, it is beneficial for achieving strong emission in LED operation, since radiative recombination between free charges has a much lower efficiency compared to excitonic recombination (free charges have a lower probability to encounter). As has been shown by Zheng et al., a significantly higher $E_b$ is found in $MAPbBr_3$ nanoparticles compared to bulk $MAPbBr_3$, leading to the increased PLQY seen in perovskite structures with reduced dimensionality.[29] In a recent study by Droseros et al., the physical processes that govern the PL emission of polycrystalline $MAPbBr_3$ films and films containing smaller crystal sizes were explored.[28] They also found enhanced PLQY for crystals with smaller size due to higher excitonic recombination and surface passivation. The quadratic dependence of the initial PL emission amplitude on the incident excitation fluence in micrometer-scale crystallites (as was found by Zheng et al.), turns into a linear dependence at small crystals sizes, agreeing with the enhanced excitonic recombination for small crystals.[29] A consequence of $E_b$ being slightly higher than the thermal energy at RT is that free charges and excitons can coexist in polycrystalline bulk $MAPbBr_3$, with their ratio depending on the excitation density. There have been several studies in halide perovskites discussing the dependence of the free carrier population on the excitation fluence and proposing a fluence-dependent conversion of free carriers into excitons according to the Saha

equation.[29],[73],[74],[56],[75],[76] For $MAPbBr_3$, Droseros et al. have investigated the excitation density dependence of the time-integrated PL emission spectra in solution-processed polycrystalline thin films (grains of a few μm size),[29] to distinguish the contributions of free charges and excitons (Figure 1 (a)). Spectral changes such as a narrowing and a red-shift are seen at higher excitation densities. To analyse the PL spectra, the sum of two Gaussian functions (Equation 1) allowed for the quantitative estimation of the interplay between the population of free charges and excitons (Figure 1 (a)).

$$I_{PL} = A \cdot e^{-\left(\frac{E-E_1}{w_1}\right)^2} + B \cdot e^{-\left(\frac{E-E_2}{w_2}\right)^2} \qquad (1)$$

$A$ and $B$ are the amplitudes, $E_1$ and $E_2$ the energies of the maximum PL intensity and $w_1$ and $w_2$ the widths of the low- and high-energy Gaussian, respectively. The agreement of the width of the low-energy Gaussian with the width of the excitonic absorption (inset of Figure 1(a)) led to the attribution of this emission to excitons. In addition, the width of the high-energy Gaussian depends on the excitation density in agreement with the Burstein-Moss model (Equation 2), relating this emission to recombination of free carriers (Figure 1 (b)).

$$\Delta E_g^{BM} = \frac{\hbar^2}{2\mu^*}(3\pi^2 n_0)^{2/3} \qquad (2)$$

In Equation 2, $\Delta E_g^{BM}$ is the change in the optical bandgap, $\mu^*$ is the exciton reduced effective mass and $\hbar$ is the reduced Planck constant.[57] From this analysis, a reduced effective mass of $0.051 \cdot m_o$ was obtained for the polycrystalline $MAPbBr_3$ films, that is lower but on the same order of magnitude with reported values in literature. [3],[32],[33],[70] The threshold where the width of the high-energy PL band starts to increase corresponds to the situation where all traps are filled with carriers, corresponding to a trap density of $7 \cdot 10^{15}$ $cm^{-3}$.[57],[77]

The energy difference between the maximum of the two Gaussian PL bands was used to estimate an $E_b$ of 110 meV, which is at the higher limit of the values reported in Table 1. Moreover, the attribution of the amplitude of each Gaussian to the population of excitons and free charges allowed to estimate the relative population of each species as a function of carrier density (Figure 1 (c)). The co-existence of free charges and excitons at low excitation densities and the conversion of free charges into excitons at higher excitation densities was revealed. This was further confirmed by the agreement of the ratio of the squared population of the free charges divided by the population of excitons with the Saha equation (equation 3, Figure 1 (d)).

$$R = \frac{n_{e,h}^2}{n_X} = \frac{1}{n}\left(\frac{2\pi\mu^* k_B T}{h^2}\right)^{3/2} e^{-\frac{E_B}{k_B T}} \qquad (3)$$

Here, $n_{e,h}$ and $n_X$ is the population of free charges and excitons respectively, both divided by their sum, which accounts for the total population. $\mu^*$ is the exciton reduced effective mass, $k_b$ is the Boltzmann constant, $h$ is the Planck constant, $T$ is the temperature in Kelvin and $E_B$ is the exciton binding energy. In agreement with this study, Liu et al. have found that the dependence of the PL intensity on the excitation density changes from quadratic to linear when increasing the excitation density,[33] thus confirming that free carriers convert into excitons. In the same line, an early work by Kunugita et al. has shown that excitons are present in $MAPbBr_3$ even at RT,[60] while the generation of both free carriers and excitons upon photoexcitation has been observed by Guo et al.[30]

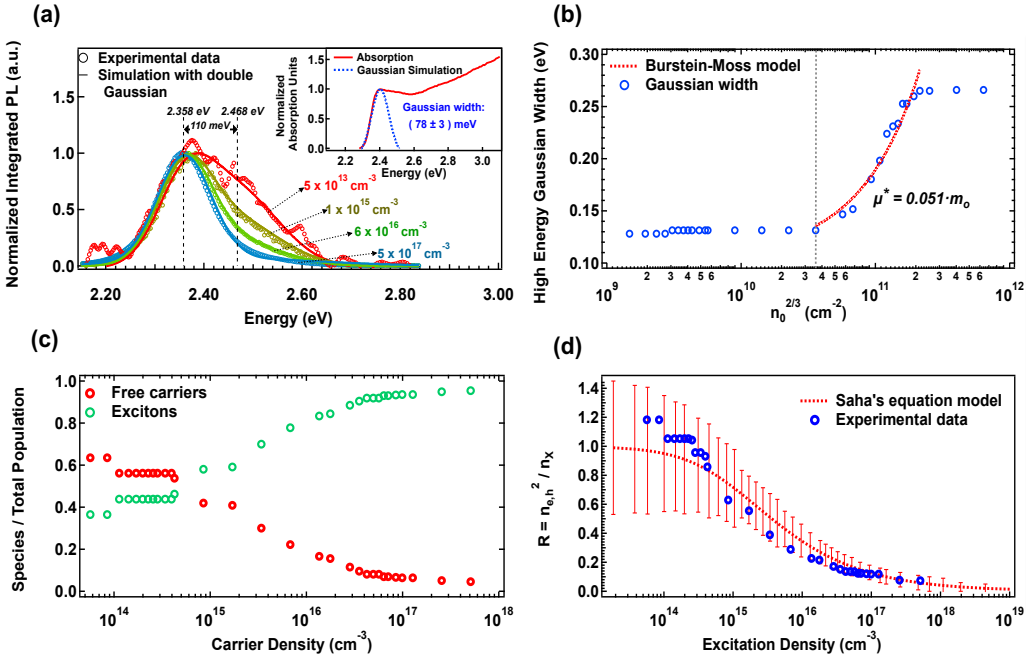


**Figure 1.** (a) Time-integrated PL spectra obtained under different excitation densities, and simulated by a double Gaussian function, for the polycrystalline $MAPbBr_3$ film. The absorption of the same sample, with the excitonic peak analysed with a single Gaussian function is shown in the inset. (b) Width of the high-energy Gaussian ($w_2$) versus $n_0^{2/3}$, analysed by the Burstein-Moss model. (c) Population of free carriers and excitons over the total population of the excited state. (d) Ratio of the squared population of free carriers, compared to the Saha equation model. Reproduced with permission for ref. [28]. Copyright © 2018, American Chemical Society.

Guo et al. have compared the results from temperature-dependent time-resolved PL (TRPL) spectroscopy and time-resolved microwave conductivity (TRMC) on a $MAPbBr_3$ single crystal at the different crystal phases (orthorhombic, tetragonal and cubic) and for different photon fluences (Figure 2).[30] PL spectroscopy is sensitive to the radiative recombination of both excitons and charges, while only the decay of free charges is obtained via TRMC. The

difference between the PL and photoconductance transients is evident in all three phases as depicted in Figure 2. More precisely, PL lifetimes differ significantly between the three phases and exhibit an intensity-dependence in the cubic phase (Figures 2 (a-c)). On the other hand, the TRMC transients (Figures 2 (d-f)) are significantly slower than the PL decays and do not exhibit any dependence on the excitation density for all three phases. These observations suggest that different species are responsible for the obtained signals and that both excitons and free charges are formed upon photoexcitation. Since in the cubic phase, the PL recombination becomes slower for higher photoexcitation densities, while the TRMC results do not show similar behaviour, the authors attribute this PL decay to exciton recombination. They have also provided evidence that the yield of charge carriers decreases at lower temperatures (more excitons are formed), because of the increased exciton binding energy in this material.

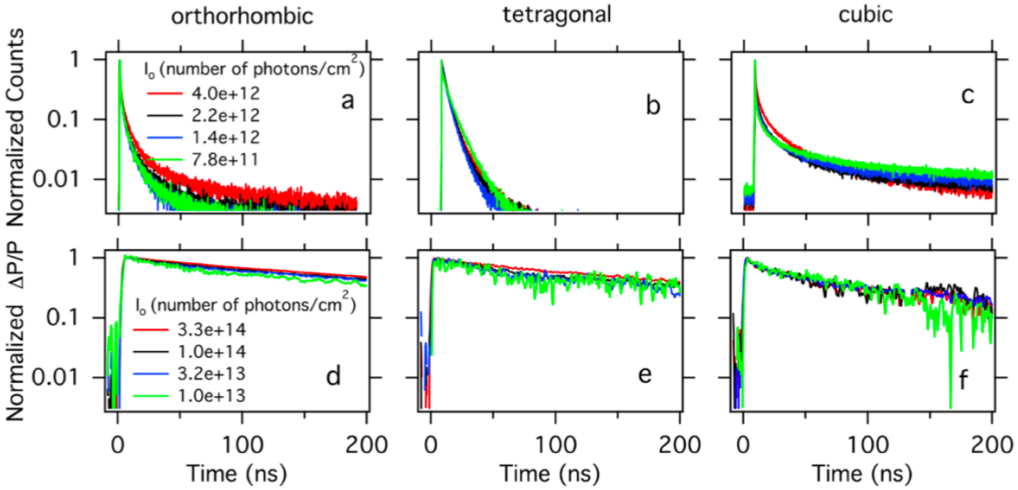


**Figure 2**. Upper panels (a-c): Normalized TRPL traces of $MAPbBr_3$ single crystals at 550 nm. Lower panels (d-f): Normalized TRMC photoconductance transients recorded with 500 nm excitation. (a,d) Orthorhombic phase, T = 90 K; (b,e) tetragonal phase, T = 210 K; (c,f) cubic phase, T = 300 K. Reproduced with permission from ref. [30] (https://pubs.acs.org/doi/abs/10.1021/acs.jpclett.7b01642), further permissions related to the material excerpted should be directed to the ACS.

Finally, Liu et al. have shown that excitons, electron-hole pairs and free carriers coexist in $MAPbBr_3$ thin films and have studied their contribution to the TRPL at different temperatures.[78] More specifically, analysing the TRPL dynamics with a sum of three exponentials has allowed to clearly disentangle the species that contribute to the PL emission. In agreement with Guo et al.,[30] they have shown an increased contribution of excitonic recombination at low temperatures, especially in the orthorhombic phase due to the higher exciton binding energy, accompanied with a decrease in the population of electron-hole pairs and free carriers. As the temperature increases, going from the orthorhombic to the tetragonal phase, the population of excitons and their PL lifetime decrease, while the population of

electron-hole pairs increases. A further increase in the temperature above the tetragonal-to-cubic phase transition then causes an evident increase in the population of the free carriers. Deviations in the trend of the time constants close to the temperatures of the three phase transitions have been attributed to the existence of shallow trap states, the nature and the population of which is suggested to be temperature-dependent.

### 2.2 Further processes affecting the PL peak position

We have seen that both excitons and free charges can contribute to the PL of $MAPbBr_3$. This is however not the only parameter affecting the emission spectrum of the material. Significant discrepancies are found in literature about the position of the PL peak with values between 500 nm and 574 nm,[79],[80],[81],[82],[83],[84] and dual PL emission has also been observed.[85],[83],[86],[87],[88] The variation in PL position and the dual PL emission have been attributed to different origins such as re-absorption, re-absorption combined with carrier diffusion,[87],[88] distinct emission from bulk and surface states (due to different bandgaps or different perovskite phases),[87],[88],[83],[89],[83],[89],[83],[90] different band energies of ordered and disordered domains,[91] and finally to a Rashba-like spin-split.[92] These phenomena are discussed below in more detail.

Re-absorption in thick crystals is an important issue that has been addressed in $MAPbBr_3$ and significantly affects the PL position, because of the strong band-to-band absorption coefficient and the small Stokes shift between the absorption and PL emission.[93] Wenger et al. have studied the optical properties of a $MAPbBr_3$ single crystal (thickness of 2.13 mm).[94] The absorption spectrum (Figure 3 (a)) shows a sharp peak at 540 nm characteristic of a strong excitonic transition, followed by continuum band absorption at higher energies that significantly increases below 550 nm. To understand the contribution from re-absorption, the PL spectrum was recorded at different configurations, by collecting once the PL that passes through the sample and once close to the photoexcited surface. As shown in Figure 3 (a), a red-shift of the PL peak is detected after passing through the crystal (red line) with respect to the light collected close to the surface (blue line), due to important re-absorption in the crystal. Figure 3 (b) shows the calculated transmitted PL emission for different thicknesses including the effect of re-absorption. As shown, when the light passes through the perovskite, a reduction of the high energy part of the PL spectrum occurs causing the red-shift of the PL peak. The calculated transmitted PL through a single crystal of the same thickness matches the experimentally measured spectrum (Figure 3 (c)). From this study, the authors excluded the

presence of a different bandgap at the surface of the single crystal with respect to the bulk, as suggested in an earlier study.[83] They further supported their conclusions by performing depth-profiling with two-photon excitation PL spectroscopy. Diad et al. have also demonstrated the important role of re-absorption on the PL spectral position by comparing their experimental spectra from depth-resolved cathodoluminescence spectroscopy with the simulated ones, and combining them with complementary steady-state and TRPL measurements.[34] Their TRPL measurements have shown a longer-lived PL emission transmitted through a $MAPbBr_3$ single crystal compared to the PL emitted close to the surface. They concluded that re-absorption of light allows for radiative transport. This is the emission of reabsorbed photons at a different location from their initial point of absorption, a dominant mechanism inside large crystals that is suggested to be responsible for the good carrier transport properties seen in $MAPbBr_3$. Furthermore, Yamada et al. took advantage of the different signal depths of one-photon and two-photon PL experiments to distinguish emission from near surface regions and deep inner bulk regions of $MAPbBr_3$.[87],[88] They assigned the high energy PL (2.35 eV) as originating from the near surface region, while the low energy PL (2.18 eV) was attributed to the bulk. A model that includes both re-absorption and carrier diffusion from the surface to the bulk was used to describe the spectral shift and the difference between the lifetime in the bulk and at the surface.

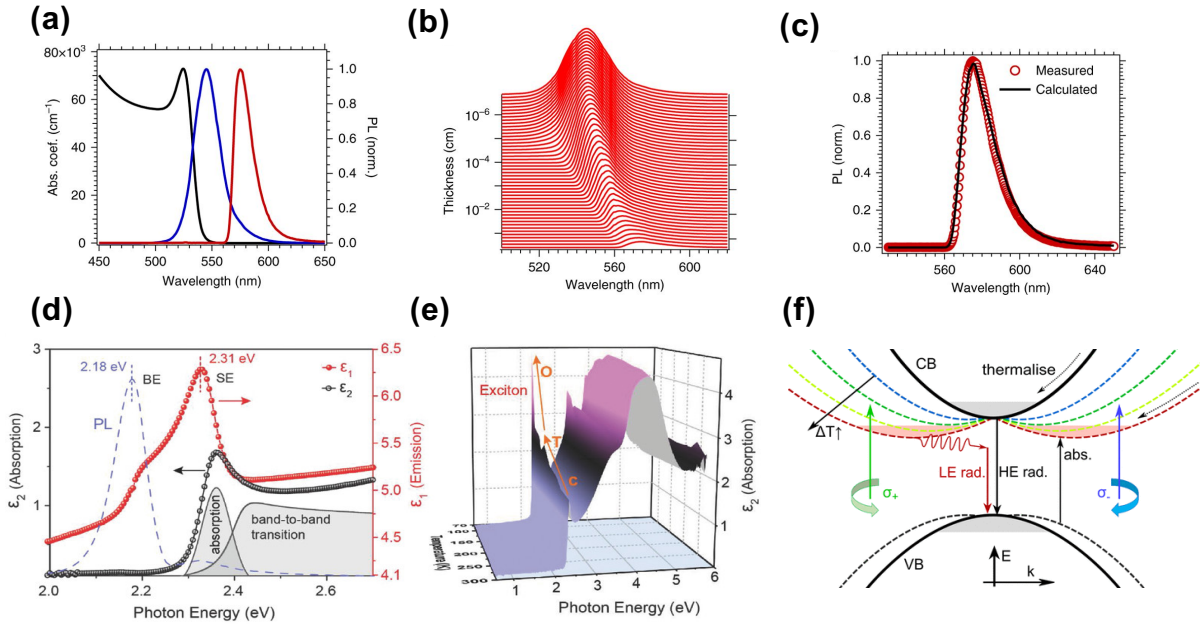


**Figure 3.** Photoluminescence (PL) spectra of single crystals of $MAPbBr_3$. **a.** Absorption and PL emission spectra collected from the front (*blue*) and from the rear (*red*) of the crystal. **b.** Calculated attenuation and shift of the PL emission throughout the thickness of a crystal by re-absorption effects. The initial PL spectrum ($d = 0$ mm) is the one obtained from the front of the crystal (*blue curve* in **a**). **c.** Comparison of the normalised PL spectra measured from the rear of the crystal (*red circles*) and that calculated including re-absorption within the bulk of the

crystal (last spectrum of **b**, with $d = 2.13$ mm). Reproduced with permission from ref. [94]. Copyright © 2017, Springer Nature. **d.** Room temperature dielectric function ($\varepsilon_1$, $\varepsilon_2$) of single crystal $MAPbBr_3$ in comparison with the PL spectrum. **e.** Temperature-dependent dielectric function of single crystal $MAPbBr_3$. Reproduced with permission from ref. [90]. Copyright © Copyright Clearance Center's RightsLink®, licence No 4678691270296. **f.** Schematic energy band structure depicting thermally driven Rashba-like spin splitting, with selective excitation provided using left ($\sigma_+$) and right ($\sigma_-$) circularly polarized light. Photogenerated carriers recombine by two main radiative (rad.) pathways: a high-energy (HE) unperturbed direct bandgap transition and a phonon-mediated low-energy (LE) indirect bandgap transition. For simplicity, only the conduction band (CB) splitting is shown with a thermal dependence. Reproduced with permission from ref. [92]. Copyright © 2019, American Chemical Society.

The process of re-absorption leads to photon recycling that has been suggested to increase the PCE of SCs,[35] because the repeated re-absorption and re-emission processes allow the building up of charge carriers in the active layer, increasing the quasi-Fermi level splitting.[36],[37] Photon recycling is defined either as a one-cycle photon re-absorption, where the radiatively emitted photons after external light excitation are absorbed again by the photoactive layer, or by multiple-cycle photon re-absorption and re-emission processes.[38],[95],[96] In addition to the small Stokes shift and strong absorption necessary for re-absorption to occur, a high internal PL quantum yield is required for high photon recycling efficiency.[97],[98] The possible contribution of photon recycling to the overall PCE of SCs, as-suggested by Diab et al.,[34] has been studied in detail by Fang et al.[38] They have found the photon recycling efficiency to be low (< 0.5%) for light intensity equal to one sun, by measuring the ratio of the recycled photons to the initially absorbed photons based on their polarization difference. This was related to the final emission intensity after multiple cycles of re-absorption and re-emission. The low photon recycling efficiency was attributed to a low PLQY in single crystals at low absorbed photon density. The authors did not exclude that higher photon recycling efficiency in polycrystalline films with different PL properties can be achieved. These results show that the long carrier diffusion length and long radiative lifetimes of perovskite single crystals are not significantly enhanced by photon recycling, highlighting their intrinsically excellent charge transport properties. Moreover, the origin for the wavelength variation of the PL peak maximum in perovskite single crystals has been investigated in detail showing that the additional lower energy peak mainly originates from the filtered PL leaking from the top surface and edges of the crystal after self-absorption and multiple reflections.

As discussed above, Diab et al.,[34] Fang et al.,[38] and Wenger et al.[94] have attributed the lower energy PL peak to re-absorption in crystals of large size. On the other hand, a recent study by Chi et al. on single crystals and also polycrystalline thin films attributes the dual PL emission in $MAPbBr_3$ to the existence of two distinct excitonic states,[90] one in the bulk and one at the

surface. Measuring the complex dielectric function using spectroscopic ellipsometry, the two states were detected at 2.18 eV and 2.31 eV as shown in Figure 3 (d). The excitonic emission from near surface regions is expected to have a higher intensity than the emission from the bulk due to the limited penetration depth of the excitation source in the ellipsometry measurements (while the opposite trend is seen in PL). On this basis, the stronger excitonic feature at 2.31 eV was assigned to originate from the surface, and the 2.18 eV feature from the bulk. Combining the evidence for the distinct PL emission from the bulk and the surface (dashed line in Figure 3 (d)) with X-ray diffraction measurements, they showed that the surface of the crystal is enriched in orthorhombic phase, while the bulk is governed by the cubic phase. Since the orthorhombic phase is only present at the surface, the high energy PL peak (2.31 eV) of the single crystal (Figure 3 (d)) has a smaller intensity compared to the low energy peak (2.18 eV) that originates from the bulk. To provide additional proof for the origin of the two peaks, the authors studied the intensity of the high energy excitonic peak when generating more orthorhombic phase in the crystal by reducing the temperature. A phase transition from cubic (C) to tetragonal (T) and finally orthorhombic (O) is known to take place in perovskites as the temperature decreases.[99],[100] Figure 3 (e) shows the temperature dependent dielectric function. An increase of the high energy peak is observed with the successive phase transitions, thus confirming the origin of the dual emission from two distinct excitons. Finally, the presence of the orthorhombic phase on the surface at RT was shown to be related to sample air-exposure, which possibly explains why the effect is not systematically observed in all reported studies. Another structure-related interpretation of the dual emission in $MAPbBr_3$ was provided by Dar et al. via temperature-dependent PL measurements supported by simulations.[91] They attributed the dual emission to the difference in bandgap between ordered and disordered domains of the perovskite, caused by a higher energy of the valence band (VB) in disordered domains with respect to ordered ones that enables the migration of photogenerated carriers from the ordered to disordered regions.

Finally, an additional electronic phenomenon that can contribute to the dual emission observed in $MAPbBr_3$ is the strong Rashba-like spin-split present in this perovskite.[101],[102],[103],[92] The combination of two phenomena leads to this effect: First, the strong SOC that is induced by the heavy Pb atom and second, a static or dynamic breaking of the inversion symmetry in the crystal that leads to the appearance of an effective magnetic field on the electrons by SOC, lifting spin degeneracy and splitting the band electronic structure.[92] How the Rashba-like effect leads to dual emission is explained by Steele et al.,[92] supported by temperature dependent PL measurements, and is schematically shown in Figure 3 (f). The effect causes the

shift of the valence band maxima (VBM)[104] and conduction band minima (CBM) away from the high symmetry points in the Brillouin zone, giving rise to low energy (LE) indirect tail states.[105],[106] As shown in the same figure, the shift for Pb-based perovskites in reciprocal space is expected to be larger for the CBM compared to that of the VBM due to the relative orbital contributions to the band structure,[107] allowing a LE indirect transition alongside the high-energy (HE) direct one. The recombination from the LE and HE to the VB then leads to the dual emission. In the same study, cation substitution by caesium (Cs) is shown not to influence the contribution of SOC to the dual emission.

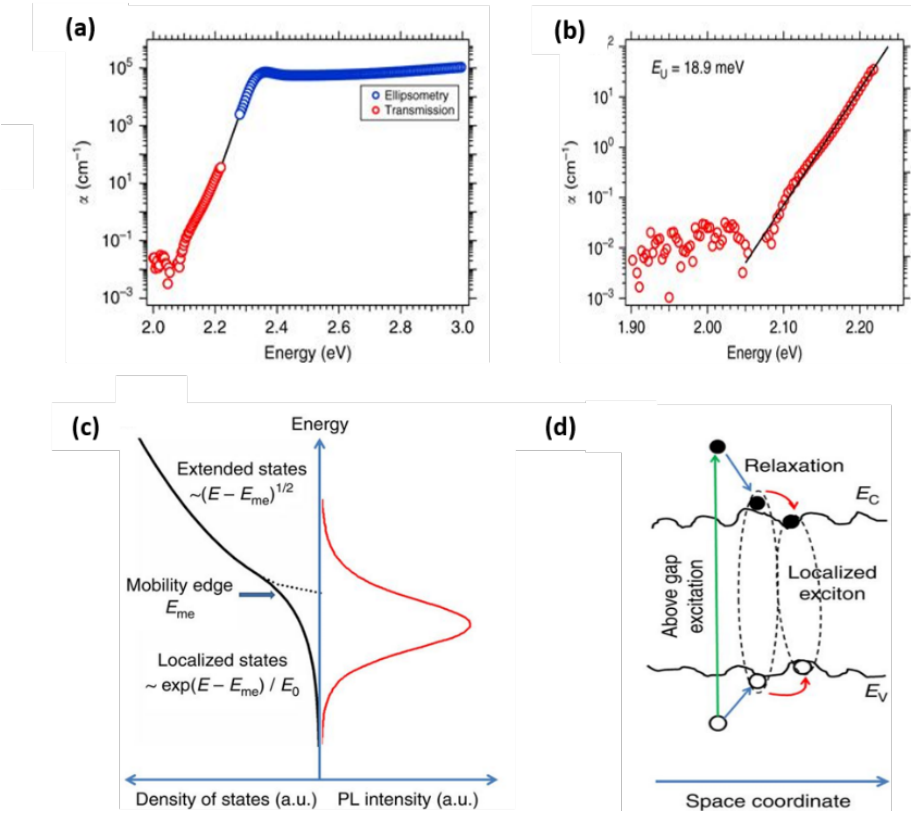


**Figure 4. a.** Absorption coefficient obtained from the combination of transmission (red circles) and ellipsometry (blue circles) data. For the transmission data, α is calculated from Beer-Lambert law (crystal thickness 2.13 mm) and for the ellipsometry data from the attenuation coefficient k. **b.** Estimation of the Urbach energy by fitting the exponential tail of the absorption spectrum. Reproduced with permission from ref. [94]. Copyright © 2017, Springer Nature. **c**. Density of the extended and localized states, and emission in perovskites (schematic). The density of the localized states is approximated by an exponential tail with the form ~exp(−$E/E_0$), where $E_0$ is the Urbach energy. The localized and extended states are separated by the mobility edge. Under low excitation density, the excitons mainly occupy the localized states. Under high excitation density, the localized states can be filled and the photocarriers also occupy the extended states, leading to emission from free carriers. **d**. Schematic drawing of exciton localization in space coordinates. With the presence of structural disorder, the tails of the localized states form local potential fluctuations in the energy bands. These potential minima can localize electrons and holes to form localized excitons. The carriers can transfer between the local potential minima, leading to long PL lifetimes. Reproduced with permission from ref. [108]. https://creativecommons.org/licenses/by/4.0/.

## 3. Disorder, Defects and Traps in $MAPbBr_3$

### 3.1. Energetic disorder and band tail states

We now turn to the impact of disorder, defects and traps on the excited-state properties of $MAPbBr_3$. Intrinsic disorder in this material manifests itself in the form of tail states in the sub-bandgap absorption (Urbach tail), and by defects that occupy states either close to the band edge or deeper in the bandgap. The exponential decay of the absorption below the energy gap can be used to evaluate energetic disorder characterized by the Urbach energy $E_u$. In cases where significant energetic disorder exists in the crystal lattice, the optical band is broadened. On the other hand, low Urbach energies are indicative for the good quality of the material and thus are desirable for semiconductors used in electronic and optoelectronic devices.

The advantage of using a perovskite single crystal is that the intrinsic disorder is estimated while minimizing the effect of surface states, as the bulk of the material has a bigger contribution than the surface.[94] According to Wenger et al.,[94] the high absorption coefficient and important thickness of $MAPbBr_3$ single crystals prohibits however the correct measurement of absorption coefficients above the energy bandgap via steady state absorption measurements (due to saturation). Therefore, ellipsometry measurements combined with absorption measurements are necessary to extract the absorption coefficient when the penetration depth is short compared to the sample thickness, as shown in Figure 4 (a). These measurements were used to estimate the Urbach energy of a $MAPbBr_3$ single crystal, by fitting the exponential tail below the bandgap with Equation 3: [94],[109]

$$\alpha(h\nu) = Ae^{\frac{h\nu}{E_u}} \qquad (3)$$

Here, $\alpha(h\nu)$ is the absorption coefficient, $h$ is Planck's constant, $\nu$ is the frequency of the detected light, $A$ is a pre-exponential factor and $E_u$ the Urbach energy. A value of $E_u$=19 meV was obtained (Figure 4 (b)). Interestingly, similar values, between 17 and 23 meV, have been found for polycrystalline $MAPbBr_3$ films showing that the intrinsic electronic disorder close to the band edge is quite small.[110],[111] The sharp optical absorption edge (low Urbach energy) is a beneficial characteristic of perovskites compared to other semiconductors such as GaAs or c-Si.[112]

He et al. have demonstrated via PL, TRPL and terahertz (THz) measurements in polycrystalline $MAPbBr_3$ films that excitons can be localized in these band tail states with a localization energy of 41 meV.[108] They have proposed the mechanism that is shown in Figure 4 (c). In this picture, the localized states are represented by an exponential tail. Thus, under low excitation

conditions, these tail states play a crucial role since most of the photocarriers occupy the localized states, while at increasing excitation density the tail states start filling up. Under excitation densities lower or close to the photovoltaic (PV) working regime ($< 5 \cdot 10^{14}$ $cm^{-3}$), the weakly bound excitons can either be partly localized (if one carrier is localized with another one Coulombically bound to it) or entirely localized.[76] At higher densities, when the tail states have filled up to a certain level, some excitons can also occupy the extended exciton states. This transition region is known as the mobility edge, approaching free excitons, as also explained in Figure 4 (d). At low excitation densities, the photoexcited excitons relax and are transferred to the localized states that in this picture are represented by local potential minima in the CB and VB. The authors have shown that excitons in these localized states have longer lifetimes than free excitons and they attribute this to the transfer between localized states.[108] In this work, a potentially beneficial role of localized excitons in light emitting applications is suggested due to their increased oscillator strength compared to free excitons.

### 3.2 Origin and density of defect states in the bandgap

The performance of perovskite materials in devices is not only affected by energetic disorder, but also by the presence of trap and/or defect states. In most cases, defects are the main reason causing non-radiative recombination that competes with radiative decay and results in a decrease of PLQY and shorter radiative lifetimes. In addition, J-V hysteresis observed in perovskite SC devices has been attributed to point defects and mobile ionic species,[113],[114],[115],[86] which result in accumulation of charges close to the crystallite boundaries and perovskite surface. Since defects play an essential role in the efficient device operation, it is important to study their origin and density.

Traps can be caused by various defects such as lead or bromide vacancies ($V_{Pb}$, $V_{Br}$), interstitials ($Pb_i$, $Br_i$) and antisites ($Pb_{Br}$, $Br_{Pb}$), while the methylammonium (MA) cation can participate in the formation of interstitials and substitutions ($MA_i$, $MA_{Pb}$).[39] Discrete absorption from defect states has been detected by Sutter-Fella et al.[117] The use of sensitive external quantum efficiency (sEQE) measurements on bromide based and other halide perovskite devices has allowed for the observation of weak sub-bandgap absorption features that are attributed to transitions from bound to free electronic states that generate the obtained photocurrent. In $MAPbBr_3$, the authors have probed two different absorption bands at 1.42 eV and 1.9 eV and related them to Pb vacancies. In addition, temperature-modulated space charge limited spectroscopy, which is an electrical method, was employed on $MAPbBr_3$ single crystals and has addressed the presence and distribution of deep trap states, with their densities found

between $10^{-9}$-$10^{-10}$ $cm^{-3}$.[118] Motti et al. have reported that the presence of oxygen can passivate the trap states formed in $MAPbBr_3$ thin films, since an increase of band-to-band PL emission and PLQY was observed after sample exposition to oxygen.[119] On the same line, a more recent study by Zhang et al. has shown that the PL intensity emitted by a $MAPbBr_3$ single crystal decreases in vacuum compared to air, accompanied by an increased conductivity.[120] This was now attributed to the reduction of shallow trap states that are caused by $O_2$ when the crystal is exposed to air, pointing to a positive role of those shallow traps for the PL. The same study shows that the PL intensity recovers upon air-exposure when the shallow traps are formed again. Employing density functional theory (DFT), the authors have identified the shallow trap states to be Frenkel defects, which are formed when a $Br^-$ anion moves into an interstitial site around Br atoms in the crystal structure, creating a vacancy.

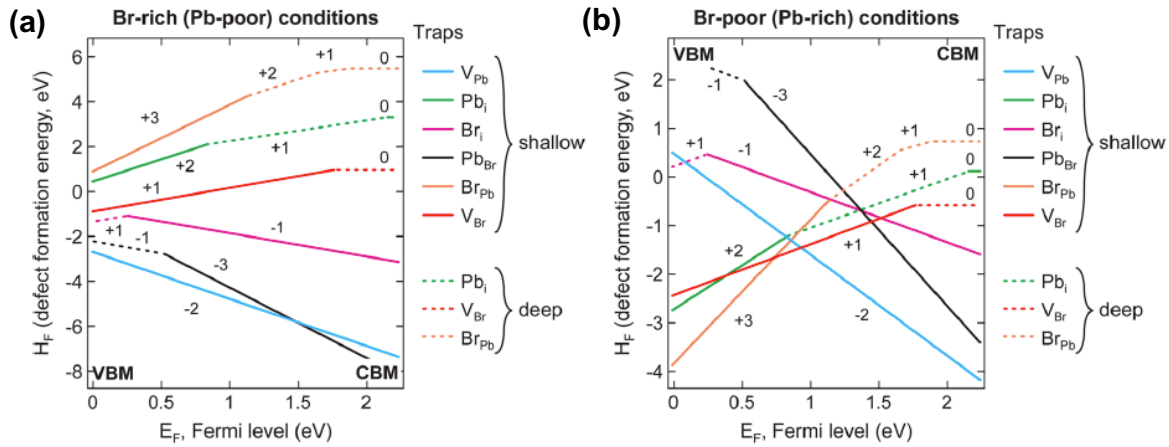


**Figure 5.** Defect formation energies under (a) halide-rich and (b) halide-poor conditions for cubic $MAPbBr_3$. Solid lines represent near-band edge states while dashed lines represent in-gap states. Reproduced with permission from ref. [116]. Copyright © 2015, American Chemical Society.

Another study by Falk et al. indicates that not only the environment, but also the stoichiometry can affect the defect formation in $MAPbBr_3$.[121] On the one hand, the PL and device performance directly after fabrication are independent on the precursor stoichiometry, while on the other hand the stoichiometry plays an important role for the long-term stability and performance. Devices prepared with under-stoichiometric conditions show a large increase of the PCE and electroluminescence quantum efficiency (ELQE) with time, when operated as SCs or LEDs, respectively. This has been attributed to an $O_2$ assisted self-healing process of the defects in Br-deficient $MAPbBr_3$.[121] Buin et al. have performed theoretical calculations in order to understand the role of the stoichiometry in $MAPbBr_3$ single crystals.[116] Figure 5 shows eigenvalues (defect formation energies), derived from first principle DFT calculations, for the

defects that can be formed under (a) Br-poor and (b) Br-rich $MAPbBr_3$ conditions for a single crystal.[116] The points of equal formation energy for different charged states indicate whether the defect states are deep or shallow, depending if they lie in the band gap or close to the band edge. The solid lines in Figure 5 represent states near the band edge, while the dashed lines are in-gap states. The stable charged states in the band gap are deep defects while the states that lie close to the band edge are shallow defects. According to the diagram, the main deep traps in this material are $Pb_i$ and $V_{Br,}$ while the halide-rich conditions favour the elimination of these deep trap centres. Under halide-rich conditions, $V_{Pb}^{-2}$ still plays a dominant role as a deep trap, but the $Pb_i$ defects become less favourable. In addition, $Pb_{Br}$ antisites in the cubic $MAPbBr_3$ phase were found to exhibit a deep-trap character associated with formation of linear $Br^{3-}$ ions. $Pb_{Br}$ is a deep acceptor with very high thermal ionization energy,[122] while $V_{Br}$ exhibits deep-trap behaviour. The interstitial defects ($Br_i$) have a negative correlation energy but only the charge state +1 is stable and close to the VBM.

In addition, Wang et al. have investigated the role of Methylamine ($MA^*$: $CH_3NH_2$), which is present upon film deposition, on the formation of defects using spin-polarized DFT.[39] Although $MA^*$ molecules are not stable, they affect the trap formation during spin-coating by penetrating into the Pb-Br matrix and forming $MA_i^*$-Br bonds. Those $MA_i^*$-Br sites form shallow level defects near the HOMO, suggested to cause an increase in the PLQY due to radiative recombination of trapped holes with LUMO electrons. Two configurations of the $MA^*$ molecules with respect to the nearest MA cation are possible: syntropy, where the N atom of $MA^*$ is aligned with the C atom of the MA cation, and reversal, where the N atom of $MA^*$ is aligned to the N atom of the MA cation. In the case of syntropy orientation, the interaction between the MA cation and $MA^*$ is negligible, so that they interact only in the reversal configuration. Figure 6 shows the participation of $MA^*$ (red line) and Pb-s (blue line) states to the total density of states (TDOS) (black line) and projected density of states (PDOSs) of the $MA^*$ molecule and nearest MA cation (purple line), for the case of $MA_i$*-Br (syntropy) and $MA_i$*-Br (reversal). For reversal orientation, $MA^*$ does not influence the band edge (as seen by the absence of MA* states for energies above zero), while for syntropy orientation the band edge is entirely determined by $MA^*$ and the s orbital of the Pb atom. The $MA_i^*$ interstitial defect can be easily removed by annealing, but MA interstitials ($MA_i$) and substitutions ($MA_{Pb}^*$) were found to be stable even after annealing.

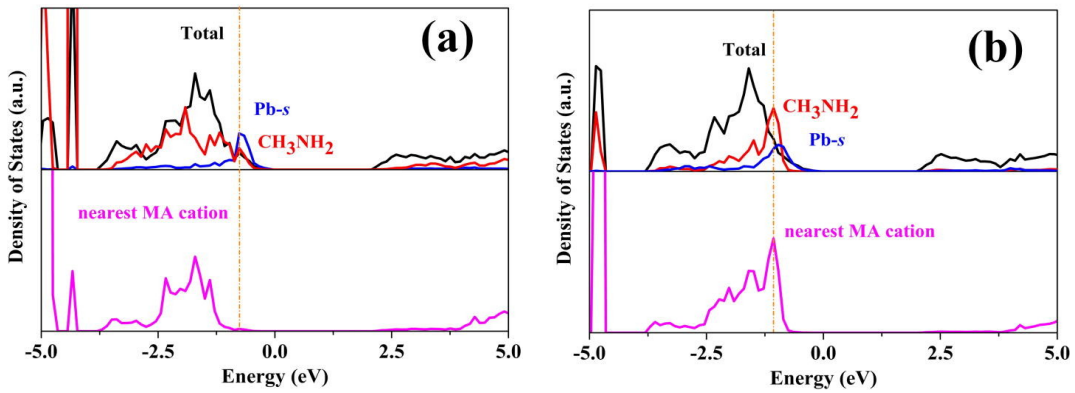


**Figure 6**. TDOS (total density of states, black line) and PDOSs (projected density of states) of **a.** $MA_i$*-Br (syntropy) and **b.** $MA_i$*-Br (reversal). Reproduced with permission from ref. [39]. Copyright © Clearance Center's RightsLink®, licence No 4678750985792.

The effect of the organic cation in bromide perovskites on the density of trap states and on ion migration has been recently investigated by Oranskaia et al., who have compared the methylammonium (MA) and formamidinium (FA) cation in stable cubic-phase bromide perovskites.[40] The authors have used DFT calculations to study the $V_{Br}$ and $Br_i$ defects. They have found that these defect states have a higher density in $MAPbBr_3$ compared to $FAPbBr_3$, for example because of a lower formation energy of $Br_i$ due to the lower cation rotation barrier in $MAPbBr_3$ that facilitates their stabilization. The higher density of point defects in $MAPbBr_3$ contributes to enhanced ion migration. This is in agreement with studies reporting that halide vacancies are highly mobile, while the cation and the lead do not contribute significantly to the ion migration.[123], [124] The lowest migration barrier of the $V_{Br}$ defects was calculated by considering all possible pathways (Figure 7) and was found to be lower in the MA based bromide perovskite (0.27 and 0.33 eV for $MAPbBr_3$ and $FAPbBr_3$, respectively).[40] This is related to the stronger H-bonding stabilization and higher rotation barrier of the organic cation in $FAPbBr_3$. The minimum energy barrier for the through-cell $V_{Br}$ migration pathway follows the same trend (0.46 eV in MAPbBr3 and 0.85 eV in FAPbBr3). This contributes to the ionic motion in $MAPbBr_3$, making Br migration through $V_{Br}$ more important than in $FAPbBr_3$.

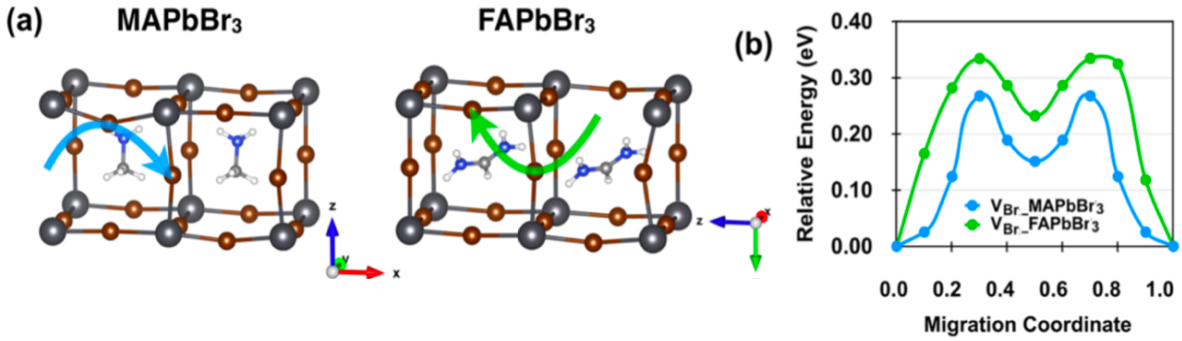


**Figure 7. a.** Bromide vacancy ($V_{Br}$) migration pathways and **b.** their energy profiles along the

migration paths in $MAPbBr_3$ and $FAPbBr_3$. Note that relative energy refers to the minimum energy of the optimized crystal structure before ion migration. Reproduced with permission from ref. [40] (https://pubs.acs.org/doi/10.1021/acs.jpclett.8b02522), further permissions related to the material excerpted should be directed to the ACS.

Finally, going to an inorganic cation, the case of caesium lead tribromide ($CsPbBr_3$) has been examined by Sebastian et al.[125] The authors have identified by DFT calculations that the most dominant defects are $V_{Cs}$, $V_{Pb}$, $Pb_{Cs}$ and $V_{Br}$, while the antisites $Pb_{Br}$ and $Cs_{Br}$ are unlikely to be formed due to their high formation energies. Interestingly, $Pb_{Cs}$ and $V_{Br}$ were found to occupy states at 0.24 and 0.23 eV above the bandgap, respectively, and to actively participate to the above-band gap PL emission of the material. This is suggested to originate from a bound exciton that is formed between an electron trapped by the $Pb_{Cs}$ or $V_{Br}$ states in the CB and a free hole in the VB.[40] The behaviour of the $V_{Br}$ trap in $CsPbBr_3$ is thus in contrast to $MAPbBr_3$, where $V_{Br}$ has a deep trap character as mentioned above. PL from an exciton bound to $V_{Br}$ has also been recently reported for $CsPbBr_3$ nanosheets,[126] confirming the results of Sebastian et al.[125] The defect tolerance of $CsPbBr_3$, especially under moderate or Br-poor conditions, has been reported by Kang et al.,[127] and it is probably the main reason for the decreased ion migration compared to hybrid organic-inorganic perovskites that employ MA as the cation.[128],[129],[130]

### 3.3 Impact of defects on the TRPL dynamics

Recently, the impact of trap/defect states on the PL dynamics of $MAPbBr_3$ has been addressed. Typical TRPL dynamics of $MAPbBr_3$ thin films show a radiative lifetime of hundreds of nanoseconds (ns), which extends to a few microseconds (μs) in single crystals.[94], [28], [131] For single crystals, re-absorption/re-emission might contribute to such long lifetimes,[94] as already discussed above. The main reason for the shortened lifetime in the polycrytalline films is however the higher concentration of defects. As shown in Figure 8 (a), the PL decay in polycrystalline films and single crystals exhibit a bi-exponential decay with a fast component (a few ns) and a slower one (hundreds of ns in films and a few μs in single crystals). The fast PL decay component was initially attributed to non-radiative recombination.[79],[82],[132] However, more recent studies show that the fast component does not originate from non-radiative recombination but from fast diffusion of carriers generated close to the point under illumination to nearby positions with a lower carrier density.[94] Therefore, the decrease of the PL intensity at early times is not due to non-radiative loss of carriers (given the low trap densities in the single crystal), but due to a reduction in the carrier density in the probed region.

The carriers that diffuse recombine radiatively at later times, so that the amplitude of the PL intensity lost at early times is compensated by the long-lived recombination of the diffused carriers. Overall, the area under the PL decay curve remains the same and the high PLQY (in single crystals) is maintained in spite of the fast decay component. The presence of carrier diffusion is further supported by the independence of the fast PL decay on the excitation fluence (it is not a bimolecular recombination process), and the red-shift of the PL emission taking place over tens of ns (Figure 8 (b) and 8 (c)), while it is in agreement with studies where carrier diffusion was used to fit the PL decay.[87],[88] A similar conclusion was reached by Guo et al. [30]

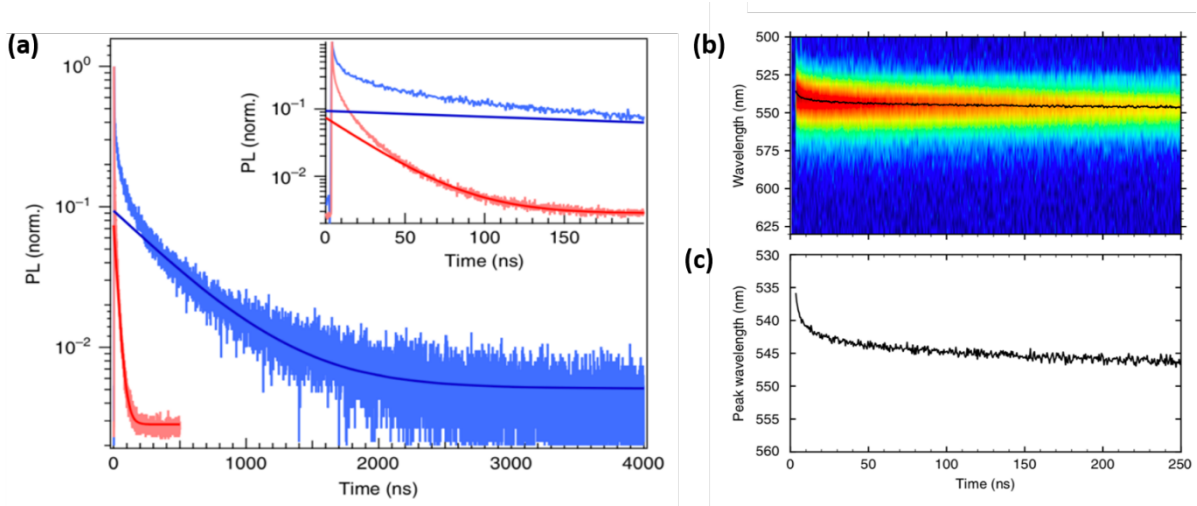


**Figure 8. a.** Normalized PL decays for $MAPbBr_3$ thin film (red) and single crystal (blue) excited at 447 nm. The tails of the decay were fit with an exponential function with constant $k_{SC} = 2.1 \times 10^6$ s$^{-1}$ and $k_{film} = 3.6 \times 10^7$ s$^{-1}$. Inset: zoom on a shorter time scale. **b.** 2D spectral map of $MAPbBr_3$ single crystal TRPL. **c.** shift of the peak centre position with time. Reproduced with permission from ref. [94]. Copyright © 2017, Springer Nature

In contrast, the difference between the long-lived lifetimes (480 ns in the single crystal and 28 ns in the polycrystalline film), as obtained by fitting the PL tails with a single exponential function (Figure 8 (a)), suggests that the trap/defect density is an order of magnitude higher in polycrystalline films compared to single crystals.[94] This long-lived PL component is influenced by the excitation fluence: it first slows down for low fluences and then fastens at higher ones as shown in Figure 9 (a) for a polycrystalline film (the same as shown in Figure 1), where the co-existence of free carriers and excitons upon photoexcitation occurs.[28] At low fluences, the PL dynamics become slower as the excitation density increases up to a value of $7 \cdot 10^{15}$ cm$^{-3}$ (Figure 9 (a)), which coincides with the density where traps are filled according to analysis with the Burstein-Moss equation (Equation 2). This situation is schematically explained in Figure 9 (b) and (c). A distribution of trap states inside the band gap, as suggested by Yamada et al.[133] and Wright et al.,[134] is considered. At low fluences, the traps are empty and thus photoexcitations gradually fill the traps (Figure 2 (b)), until the PL dynamics is

governed by band-to-band recombination. First, the trap states that lie deep in the bandgap (and which cause non-radiative recombination) are filled. As the excitation densities increase, more traps are filled including shallow trap states (Figure 9 (c)). The suggested timescale for the trapping (a few ps) is in line with TA measurements as will be shown in the next section.[135] Chirvony et al. showed that carriers temporarily trapped in the shallow states can be thermally de-trapped to re-occupy band states that contribute to band-to band PL emission, leading to delayed PL and explaining the long-lived (hundreds of ns) tail in the PL dynamics at the intermediate fluences.[136] The situation of slowest PL decay is the condition where all traps are filled, providing a good indication about the trap density. This coincides with the threshold density before the width of the high-energy PL band (free charge emission) starts to increase in Figure 1 (b). When increasing the excitation density above this threshold, the dynamics become faster (inset of Figure 9 (a)), due to higher order recombination effects, such as bimolecular and Auger recombination. Similar trends have been observed in other studies.[133], [137], [138], [139]

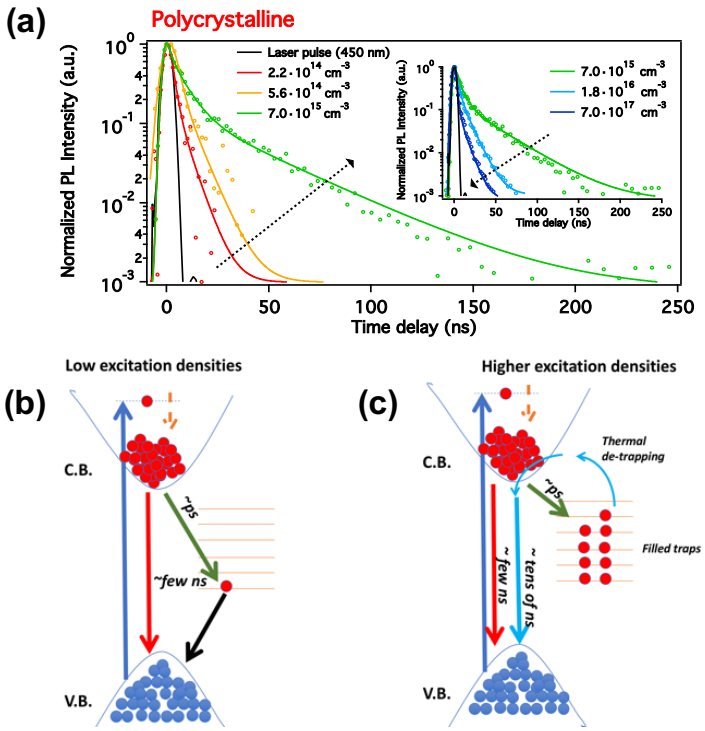


**Figure 9. a.** TRPL dynamics of a polycrystalline $MAPbBr_3$ film obtained at different excitation densities with excitation at 450 nm using pulses of 3 ns duration and a repetition rate of 10 Hz. The insets show the PL dynamics recorded at high excitation densities where the dependence of the lifetime on the excitation density is opposite to that observed at low densities. The arrows indicate an increase in the excitation density. The suggested model that explains the recombination in $MAPbBr_3$ is shown in **b.** for low and in **c.** for high excitation densities. Reproduced with permission from ref. [28]. Copyright © 2018, American Chemical Society.

## 4. Ultrafast TA dynamics of $MAPbBr_3$

To obtain information about the dynamics of photoexcited carries at early times upon photoexcitation, femtosecond transient absorption spectroscopy is commonly used. This method has been extensively applied to $MAPbI_3$,[140],[141],[142],[143],[144],[145],[146] and more recently also to $MAPbBr_3$. The ultrafast TA dynamics of hot free carriers and excitons have been studied for example by Deng et al.[135] Figure 10 (a) shows the absorption coefficient and the steady-state PL of the studied spin-coated $MAPbBr_3$ film that shows the characteristic excitonic absorption and small Stokes shift. After photoexcitation with 400 nm pulses at a relatively high excitation density of $2 \cdot 10^{18}$ $cm^{-3}$, negative photo-bleaching (PB) and positive photoinduced absorption (PA) features are present in the TA spectra, as shown in Figures 10 (b) and (c). The negative feature ($PB_1$) present close to the optical gap at 534 nm is assigned to ground state bleaching arising from electrons that have been promoted to the CB, leaving the VB depleted from carriers. Furthermore, a narrow positive peak ($PA_1$) at around 507 nm, a negative $PB_2$ band between 580 nm and 650 nm and a weak broad positive band ($PA_2$) at 715 nm are present.

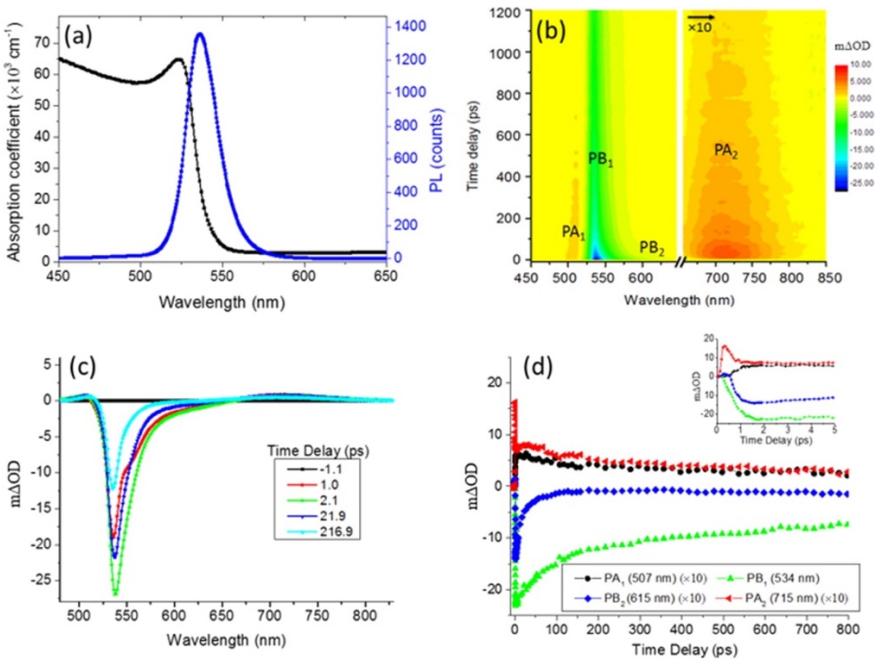


**Figure 10. a.** Absorption coefficient (black) and steady-state PL spectrum (blue) of the $MAPbBr_3$ film. **b**. Two-dimensional pseudo-color map of the TA spectra expressed in mΔOD as a function of both delay time and probe wavelength for the $MAPbBr_3$ film excited with a pump wavelength of 400 nm and fluence of 50 $\mu J/cm^2$. **c.** Evolution-associated difference (EAD) spectra of the sample (with TA spectra at −1.1 ps as baseline). **d**. Kinetic traces extracted from **b.** at indicated probe wavelengths (the inset shows kinetic traces in a short time window). Reproduced with permission from ref. [135]. Copyright © 2016, American Chemical Society.

The differences in the dynamics detected at different bands can provide more information about the processes that take place in each case. Three exponential components, one rising up to a few ps, one decaying in hundreds of ps and a slow decay that exceeds the time window of the measurement, are necessary to fit the dynamics of $PB_1$ (Figure 10 (d)). Because 400 nm is used as photoexcitation wavelength, carriers with excess energy are generated and then carrier thermalization to the band edge occurs by longitudinal optical (LO) phonon scattering, resulting in state filling at the bottom of the CB and top of the VB.[57],[55] The rise component (of a few hundred fs to ps) slows down with excitation density, confirming that fast hot-carrier cooling occurs at these times, slowing down at higher excitation densities due to a phonon bottleneck.[147],[148],[149] The faster decay component (tens to hundreds of ps depending on the excitation density) is influenced by phonon scattering and Auger processes. However, there is a debate about the origin of this recombination mechanism, since Zhang et al. have suggested that it is related to trap-assisted recombination (Figure 9 (b)).[131] On the other hand, the long decay component (ns timescale) is often assigned to free electron-hole recombination. However, as discussed above based on the TRPL measurements, this component might also originate from diffusion of carriers out of the probed region, since band-to-band recombination occurs at even slower times and is therefore not measurable by femtosecond TA. [94],[30] A weak and broad $PB_2$ band is probed below the band edge, which is assigned to trap states that are populated after photoexcitation. Thus, a negative signal is obtained that exhibits a faster recovery compared to $PB_1$ and confirms the trapping dynamics of a few tens of picoseconds (Figure 9 (b) and (c)). These sub-bandgap states have been observed for bulk $MAPbBr_3$ and nanoparticles (NPs), using above and below bandgap excitation.[150] $PA_1$ has a similar growth and decay dynamics as $PB_1$ and thus is assigned to the same origin. However, due to the differences in the rise times between $PA_1$ and $PA_2$, the authors propose that the two bands have a different origin despite the fact that the decay dynamics is similar.[135] They attribute the $PA_2$ band to photoinduced absorption from excitons. Nevertheless, this is ambiguous, since $PA_2$ overlaps with $PB_2$ from the trap states.

As discussed in section 2.1, excitons and free carriers can co-exist in $MAPbI_3$. Sharma et al. have confirmed this co-existence and have demonstrated the screening of excitons by free carriers at high excitation fluences in TA measurements,[151] showing an exciton binding energy higher than the thermal energy, in agreement with other studies.[29], [30], [60] Furthermore, another study by Zheng et al. supports the long-lived presence of excitons that decay through a first-order recombination process while co-existing with free charges.[150] On the other hand, Katayama et al. claim that an exciton binding energy for $MAPbBr_3$ higher than the thermal

energy cannot justify the good performance of $MAPbBr_3$ nanoparticles in devices,[152] as the exciton binding energy is expected to be even higher than in the bulk. They support this claim with fs-TA and TRPL measurements on $MAPbBr_3$ NPs with 5.5 nm diameter, whereby TRPL shows a biexciton feature with 21 meV binding energy that decays with a 55 ps time constant, while fast exciton quenching (~200 fs) is observed in their TA spectra. The agreement of this time constant with the one previously reported for the 'wobbling-in-a-cone' motion of the MA cation in $MAPbI_3$ perovskite (~300 fs) by Mattoni et al.,[153] led them to correlate the two processes. The oriental motion of the MA cation was suggested to be responsible for an increase in the dielectric constant of the NPs, leading to a Coulombic screening between the electron and the hole. We note here that the suggested binding energy is smaller than the thermal energy even for the NPs, which is in stark contrast with the high exciton binding energies that have been reported for 8 nm $MAPbBr_3$ NPs,[29] the observation of strong quantum confinement effects in $MAPbBr_3$ NPs with diameters varying from 3.3 nm to 7.1 nm,[154] and generally the values reported in Table 1.

## 5. Conclusion and Outlook

$MAPbBr_3$ is the most studied 3D perovskite for light emitting applications due to its strong green emission and its favourable thin film processing properties. Its high bandgap prevents its use in single junction SCs, but the current progress on its co-sensitisation has led to the achievement of very high efficiencies in multi-junction PV devices.[155, 156] In the present Progress Report, we have summarized the recent advances in the understanding of the photophysical properties of $MAPbBr_3$.

Although free carriers, excitons, energetic disorder and defects all influence the absorption of light, leading to characteristic signatures in the absorption spectrum, it is not clear how they impact on the light emission from this material. The exciton binding energy needs to be systematically determined for $MAPbBr_3$ single crystals and thin films from different preparation conditions, since this determines the extent of excitonic PL. The reported values of exciton binding energies spread over a broad range, with most of them being higher than the thermal energy at RT and the exciton binding energy reported for $MAPbI_3$. This gives rise to excitonic effects in the bromide perovskite. The co-existence of free carriers with excitons has been demonstrated in several studies, leading to additional spectral features in the emission spectrum and influencing the dynamics in ultrafast transient absorption (TA) measurements. Concerning the intrinsic energetic disorder, the reported Urbach energies show that the band edge is steep and that the disorder present in the material is low. Nevertheless, the residual

disorder affects photogenerated excitons, either by keeping them bound and thus reducing their mobility at low excitation densities, or by contributing to their long lifetimes via transfer between localized states. Although intrinsic defects are present at low concentrations in $MAPbBr_3$, they play a double role in the excited state dynamics of this system. On the one hand, they contribute to longer PL lifetimes through a trapping-detrapping process or increase the PL quantum yield by acting as hole traps that serve as radiative recombination centres with CB electrons. On the other hand, some reports show that deep traps can act as non-radiative recombination centres decreasing the PL and quantum yield and lifetime. Moreover, point defects can facilitate ion migration, a negative parameter for device performance that can be improved by cation substitution, as shown for formamidinium lead tribromide ($FAPbBr_3$).

As discussed in this report, despite the numerous studies that have been performed, the main recombination mechanism that leads to the dual emission and the long PL lifetime in single crystal $MAPbBr_3$ cannot be attributed to a single process. It seems that a plethora of different phenomena contribute, leading to the assignment of the dual emission to different mechanisms in different studies. It is thus debated whether the processes of re-absorption, photon recycling, carrier diffusion, trapping-detrapping or the Rashba effect lead to the long PL lifetime in $MAPbBr_3$ and if they can increase the PL quantum yield in thin films and single crystals. In a recent theoretical study by deQuilettes et al.,[157] the effects of trap-assisted recombination, polaron formation, Rashba effect (leading to an indirect bandgap) and of photon recycling were examined in detail. It was concluded that photon recycling and polaron formation dominate the recombination mechanism. Multiple trapping-detrapping was excluded based on the observation that both the mobility and the bimolecular rate increase when the temperature is decreased. In the same study, but also in the studies of Richter et al.[46] and Sarritzu et al.[158] it was shown that the PL emission originates from a direct bandgap transition (and not an indirect bandgap due to Rashba splitting). Given the discrepancies that exist between the various theoretical and experimental studies, a clear picture of the recombination in $MAPbBr_3$, that is generally applicable to different samples and measuring conditions, is however still lacking.

Finally, in spite of the improvement of the PL quantum yield of 3D $MAPbBr_3$, the current scientific interest has focused on perovskites with lower dimensionality, such as quasi-2D, 2D and quantum dot samples. Here, their higher exciton binding energy, band gap tunability and improved device stability favour them for light emitting applications. Nevertheless, $MAPbBr_3$ is still an ideal semiconductor for the study of many different optical phenomena and their understanding is necessary to explain the photophysics of lower dimensionality perovskites and

to achieve higher device efficiencies in multi-junction SCs in combination with lower bandgap perovskites or silicon.

Received:
Revised:
Published online:

**Biographies**

**Nikolaos Droseros** obtained his degree in Physics and a M.Sc. in Photonics from the Physics Department of the University of Patras, Greece, in 2012 and 2015 respectively. He then joined the Banerji group in the Chemistry Department of the University of Fribourg as a PhD student. Currently he continues his studies in the same group in the Department of Chemistry and Biochemistry of the University of Bern. His research interests include the photophysics and transport properties of perovskites and organic semiconductors.

**Demetra Tsokkou** is currently a Post-Doctoral Researcher in the Department of Chemistry and Biochemistry of the University of Bern. Her research aims to understand the photophysical

properties in new generation semiconducting materials. She studied Physics at the University of Cyprus and obtained her M.Sc. and Ph.D. from the same university working with Prof. Andreas Othonos on the synthesis and ultrafast characterization of semiconducting nanowires. She joined the Banerji group as a Post-Doctoral Researcher in February 2015 in the Chemistry Department of the University of Fribourg and then moved to University of Bern. She uses ultrafast laser spectroscopy to probe the photophysical and local transport properties of organic and inorganic materials.

**Natalie Banerji** is currently a Full Professor of Chemistry at the University of Bern. Her research interests include the study of organic and hybrid materials using ultrafast spectroscopic techniques, in view of solar cell and bioelectronic applications. She studied chemistry at the University of Geneva and obtained her Ph.D. degree in physical chemistry in 2009 under the supervision of Prof. Eric Vauthey. She then moved to the University of California in Santa Barbara (USA) to work on organic solar cells during a postdoctoral stay with Nobel Laureate Prof. Alan J. Heeger (2009–2011). In 2011, she started her independent research career in Switzerland at the Ecole Polytechnique Férérale de Lausanne (EPFL) with an Ambizione Fellowship by the Swiss National Science Foundation (SNSF). She moved to the University of Fribourg in 2014 as Assistant Professor, was subsequently nominated Associate Professor in 2015, and presided the Chemistry Department in Fribourg from 2016 to 2017, before moving to the University of Bern as Full Professor in 2017. She was awarded the Grammaticakis-Neumann Prize by the Swiss Chemical Society and obtained an ERC Starting Grant in 2016.

## References


[1] J. Calabrese, N. L. Jones, R. L. Harlow, N. Herron, D. L. Thorn, Y. Wang, *J. Am. Chem. Soc.* **1991**, *113*, 2328.

[2] G. C. Papavassiliou, I. B. Koutselas, *Synth. Met.* **1995**, *71*, 1713.

[3] K. Tanaka, T. Takahashi, T. Ban, T. Kondo, K. Uchida, N. Miura, *Solid State Commun.* **2003**, *127*, 619.

[4] M. Kojima, A.; Teshima, K.; Shirai, Y.; Tsutomu, *J. Am. Chem. Soc.* **2009**, *131*, 6050.

[5] H. Mehdi, A. Mhamdi, R. Hannachi, A. Bouazizi, *RSC Adv.* **2019**, *9*, 12906.

[6] S. Wang, Y. Jiang, E. J. Juarez-Perez, L. K. Ono, Y. Qi, *Nat. Energy* **2016**, *2*, 16195.

[7] R. K. Misra, L. Ciammaruchi, S. Aharon, D. Mogilyansky, L. Etgar, I. Visoly-Fisher, E. A. Katz, *ChemSusChem* **2016**, *9*, 2572.

[8] R. K. Misra, S. Aharon, B. Li, D. Mogilyansky, I. Visoly-Fisher, L. Etgar, E. A. Katz, *J. Phys. Chem. Lett.* **2015**, *6*, 326.

[9] R. Sheng, A. Ho-Baillie, S. Huang, S. Chen, X. Wen, X. Hao, M. A. Green, *J. Phys. Chem. C* **2015**, *119*, 3545.

[10] J. H. Heo, D. H. Song, S. H. Im, *Adv. Mater.* **2014**, *26*, 8179.

[11] A. Polman, M. Knight, E. C. Garnett, B. Ehrler, W. C. Sinke, *Science*. **2016**, *352*, 307, DOI 10.1126/science.aad4424.

[12] Y.-H. Kim, H. Cho, J. H. Heo, T.-S. Kim, N. Myoung, C.-L. Lee, S. H. Im, T.-W. Lee, *Adv. Mater.* **2015**, *27*, 1248.

[13] Z.-K. Tan, R. S. Moghaddam, M. L. Lai, P. Docampo, R. Higler, F. Deschler, M. Price, A. Sadhanala, L. M. Pazos, D. Credgington, F. Hanusch, T. Bein, H. J. Snaith, R. H. Friend, *Nat. Nanotechnol.* **2014**, *9*, 1.

[14] J. C. Yu, D. Bin Kim, G. Baek, B. R. Lee, E. D. Jung, S. Lee, J. H. Chu, D.-K. Lee, K. J. Choi, S. Cho, M. H. Song, *Adv. Mater.* **2015**, *27*, 3492.

[15] J. Wang, N. Wang, Y. Jin, J. Si, Z.-K. Tan, H. Du, L. Cheng, X. Dai, S. Bai, H. He, Z. Ye, M. L. Lai, R. H. Friend, W. Huang, *Adv. Mater.* **2015**, *27*, 2311.

[16] G. Li, Z.-K. Tan, D. Di, M. L. Lai, L. Jiang, J. H.-W. Lim, R. H. Friend, N. C. Greenham, *Nano Lett.* **2015**, *15*, 2640.

[17] N. K. Kumawat, A. Dey, K. L. Narasimhan, D. Kabra, *ACS Photonics* **2015**, *2*, 349.

[18] R. L. Z. Hoye, M. R. Chua, K. P. Musselman, G. Li, M.-L. Lai, Z.-K. Tan, N. C. Greenham, J. L. MacManus-Driscoll, R. H. Friend, D. Credgington, *Adv. Mater.* **2015**, *27*, 1414.

[19] V. Prakasam, D. Tordera, H. J. Bolink, G. Gelinck, *Adv. Opt. Mater.* **2019**, *0*, 1900902.

[20] M. Jäckle, H. Linnenbank, M. Hentschel, M. Saliba, S. G. Tikhodeev, H. Giessen, *Opt. Mater. Express* **2019**, *9*, 2006.

[21] H. Cho, S.-H. Jeong, M.-H. Park, Y.-H. Kim, C. Wolf, C.-L. Lee, J. H. Heo, A. Sadhanala, N. Myoung, S. Yoo, S. H. Im, R. H. Friend, T.-W. Lee, *Science.* **2015**, *350*, 1222.

[22] R. Godin, X. Ma, S. González-Carrero, T. Du, X. Li, C. T. Lin, M. A. McLachlan, R. E. Galian, J. Pérez-Prieto, J. R. Durrant, *Adv. Opt. Mater.* **2018**, *6*, 1.

[23] A. Kojima, M. Ikegami, K. Teshima, T. Miyasaka, *Chem. Lett.* **2012**, *41*, 397.

[24] L.-C. Chen, Z.-L. Tseng, D.-W. Lin, Y.-S. Lin, S.-H. Chen, *Nanomater.* **2018**, *8*, 459.

[25] G. Longo, M.-G. La-Placa, M. Sessolo, H. J. Bolink, *ChemSusChem* **2017**, *10*, 3788.

[26] M.-G. La-Placa, G. Longo, A. Babaei, L. Martínez-Sarti, M. Sessolo, H. J. Bolink, *Chem. Commun.* **2017**, *53*, 8707.

[27] Z. Xiao, R. A. Kerner, L. Zhao, N. L. Tran, K. M. Lee, T. W. Koh, G. D. Scholes, B. P. Rand, *Nat. Photonics* **2017**, *11*, 108.

[28] N. Droseros, G. Longo, J. C. Brauer, M. Sessolo, H. J. Bolink, N. Banerji, *ACS Energy Lett.* **2018**, *3*, 1458.

[29] K. Zheng, Q. Zhu, M. Abdellah, M. E. Messing, W. Zhang, A. V. Generalov, Y. Niu,

L. Ribaud, S. E. Canton, T. T. Pullerits, *J. Phys. Chem. Lett.* **2015**, *6*, 2969.

[30] D. Guo, D. Bartesaghi, H. Wei, E. M. Hutter, J. Huang, T. J. Savenije, *J. Phys. Chem. Lett.* **2017**, *8*, 4258.

[31] K.-H. Wang, L.-C. Li, M. Shellaiah, K. Wen Sun, *Sci. Rep.* **2017**, *7*, 13643.

[32] K. Galkowski, A. Mitioglu, A. Miyata, P. Plochocka, O. Portugall, G. E. Eperon, J. T.-W. Wang, T. Stergiopoulos, S. D. Stranks, H. J. Snaith, R. J. Nicholas, *Energy Environ. Sci.* **2015**, *9*, 962.

[33] Y. Liu, J. Wang, N. Zhu, W. Liu, C. Wu, C. Liu, L. Xiao, Z. Chen, S. Wang, *Opt. Lett.* **2019**, *44*, 3474.

[34] H. Diab, C. Arnold, F. Lédée, G. Trippé-Allard, G. Delport, C. Vilar, F. Bretenaker, J. Barjon, J.-S. S. Lauret, E. Deleporte, D. Garrot, *J. Phys. Chem. Lett.* **2017**, *8*, 2977.

[35] J. M. Richter, M. Abdi-Jalebi, A. Sadhanala, M. Tabachnyk, J. P. H. Rivett, L. M. Pazos-Outón, K. C. Gödel, M. Price, F. Deschler, R. H. Friend, *Nat. Commun.* **2016**, *7*, 13941.

[36] E. Yablonovitch, *Science (80-. ).* **2016**, *351*, 1401.

[37] A. W. Walker, O. Höhn, D. N. Micha, B. Bläsi, A. W. Bett, F. Dimroth, *IEEE J. Photovoltaics* **2015**, *5*, 1636.

[38] Y. Fang, H. Wei, Q. Dong, J. Huang, *Nat. Commun.* **2017**, *8*, 1.

[39] J. Wang, A. Zhang, J. Yan, D. Li, Y. Chen, *Appl. Phys. Lett.* **2017**, *110*, 123903.

[40] A. Oranskaia, J. Yin, O. M. Bakr, J.-L. Brédas, O. F. Mohammed, *J. Phys. Chem. Lett.* **2018**, *9*, 5474.

[41] M. M. Lee, J. Teuscher, T. Miyasaka, T. N. Murakami, H. J. Snaith, *Science.* **2012**, *338*, 643.

[42] D. Yang, T. Sano, Y. Yaguchi, H. Sun, H. Sasabe, J. Kido, *Adv. Funct. Mater.* **2019**, *29*, 1807556.

[43] J. Tong, Z. Song, D. H. Kim, X. Chen, C. Chen, A. F. Palmstrom, P. F. Ndione, M. O.

Reese, S. P. Dunfield, O. G. Reid, J. Liu, F. Zhang, S. P. Harvey, Z. Li, S. T. Christensen, G. Teeter, D. Zhao, M. M. Al-Jassim, M. F. A. M. van Hest, M. C. Beard, S. E. Shaheen, J. J. Berry, Y. Yan, K. Zhu, *Science.* **2019**, *364*, 475.

[44] K. Lin, J. Xing, L. N. Quan, F. P. G. de Arquer, X. Gong, J. Lu, L. Xie, W. Zhao, D. Zhang, C. Yan, W. Li, X. Liu, Y. Lu, J. Kirman, E. H. Sargent, Q. Xiong, Z. Wei, *Nature* **2018**, *562*, 245.

[45] W. Xu, Q. Hu, S. Bai, C. Bao, Y. Miao, Z. Yuan, T. Borzda, A. J. Barker, E. Tyukalova, Z. Hu, M. Kawecki, H. Wang, Z. Yan, X. Liu, X. Shi, K. Uvdal, M. Fahlman, W. Zhang, M. Duchamp, J.-M. Liu, A. Petrozza, J. Wang, L.-M. Liu, W. Huang, F. Gao, *Nat. Photonics* **2019**, *13*, 418.

[46] J. M. Richter, K. Chen, A. Sadhanala, J. Butkus, J. P. H. Rivett, R. H. Friend, B. Monserrat, J. M. Hodgkiss, F. Deschler, *Adv. Mater.* **2018**, *30*, 1803379.

[47] J. Even, L. Pedesseau, C. Katan, *J. Phys. Chem. C* **2014**, *118*, 11566.

[48] Y. Yamada, T. Nakamura, M. Endo, A. Wakamiya, Y. Kanemitsu, *IEEE J. Photovoltaics* **2015**, *5*, 401.

[49] Q. Lin, A. Armin, R. Chandra, R. R. C. R. Nagiri, P. L. Burn, P. Meredith, *Nat. Photonics* **2014**, *9*, 106.

[50] F. Ruf, M. F. Aygüler, N. Giesbrecht, B. Rendenbach, A. Magin, P. Docampo, H. Kalt, M. Hetterich, *APL Mater.* **2019**, *7*, 31113.

[51] M. Saba, M. Cadelano, D. Marongiu, F. Chen, V. Sarritzu, N. Sestu, C. Figus, M. Aresti, R. Piras, A. Geddo Lehmann, C. Cannas, A. Musinu, F. Quochi, A. Mura, G. Bongiovanni, *Nat. Commun.* **2014**, *5*, 1.

[52] N. Sestu, M. Cadelano, V. Sarritzu, F. Chen, D. Marongiu, R. Piras, M. Mainas, F. Quochi, M. Saba, A. Mura, G. Bongiovanni, *J. Phys. Chem. Lett.* **2015**, *6*, 4566.

[53] A. Miyata, A. Mitioglu, P. Plochocka, O. Portugall, J. T. W. Wang, S. D. Stranks, H. J. Snaith, R. J. Nicholas, *Nat. Phys.* **2015**, *11*, 582.

[54] S. D. Stranks, S. D. Stranks, G. E. Eperon, G. Grancini, C. Menelaou, M. J. P. Alcocer, T. Leijtens, L. M. Herz, A. Petrozza, H. J. Snaith, *Science* **2014**, *342*, 341.

[55] G. Xing, N. Mathews, S. S. Lim, Y. M. Lam, S. Mhaisalkar, T. C. Sum, S. Sun, S. S. Lim, Y. M. Lam, M. Grätzel, S. Mhaisalkar, T. C. Sum, M. Gratzel, S. Mhaisalkar, T. C. Sum, *Science.* **2013**, *342*, 344.

[56] V. D'Innocenzo, G. Grancini, M. J. P. Alcocer, A. R. S. Kandada, S. D. Stranks, M. M. Lee, G. Lanzani, H. J. Snaith, A. Petrozza, *Nat. Commun.* **2014**, *5*, 3586.

[57] J. S. Manser, P. V. Kamat, *Nat. Photonics* **2014**, *8*, 737.

[58] A. Filippetti, P. Delugas, A. Mattoni, *J. Phys. Chem. C* **2014**, *118*, 24843.

[59] Y. Jiang, X. Wang, A. Pan, *Adv. Mater.* **2019**, *31*, 1.

[60] H. Kunugita, T. Hashimoto, Y. Kiyota, Y. Udagawa, Y. Takeoka, Y. Nakamura, J. Sano, T. Matsushita, T. Kondo, T. Miyasaka, K. Ema, *Chem. Lett.* **2015**, *44*, 852.

[61] F. Zhang, H. Zhong, C. Chen, X. Wu, X. Hu, H. Huang, J. Han, B. Zou, Y. Dong, *ACS Nano* **2015**, *9*, 4533.

[62] T. Thu Ha Do, A. Granados del Águila, C. Cui, J. Xing, Z. Ning, Q. Xiong, *Phys. Rev. B* **2017**, *96*, 075308.

[63] S. Rana, K. Awasthi, S. S. Bhosale, E. W.-G. Diau, N. Ohta, *J. Phys. Chem. C* **2019**, *123*, 19927.

[64] R. Comin, G. Walters, E. S. Thibau, O. Voznyy, Z.-H. Lu, E. H. Sargent, *J. Mater. Chem. C* **2015**, *3*, 8839.

[65] J. Shi, H. Zhang, Y. Li, J. Jasieniak, Y. Li, H. Wu, Y. Luo, D. Li, Q. Meng, *Energy Environ. Sci.* **2018**, 11.

[66] Y. Yang, M. Yang, Z. Li, R. Crisp, K. Zhu, M. C. Beard, *J. Phys. Chem. Lett.* **2015**, *6*, 4688.

[67] M. Saba, F. Quochi, A. Mura, G. Bongiovanni, *Acc. Chem. Res.* **2016**, *49*, 166.

[68] M. Hu, C. Bi, Y. Yuan, Z. Xiao, Q. Dong, Y. Shao, J. Huang, *Small* **2015**, *11*, 2164.

[69] A. M. Soufiani, F. Huang, P. Reece, R. Sheng, A. Ho-baillie, M. A. Green, *Appl. Phys. Lett.* **2015**, *231902*, 1.

[70] I. B. Koutselas, L. Ducasse, G. C. Papavassiliou, *J. Phys. Condens. Matter* **1996**, *8*, 1217.

[71] M. Bokdam, T. Sander, A. Stroppa, S. Picozzi, D. D. Sarma, C. Franchini, G. Kresse, *Sci. Rep.* **2016**, *6*, 1.

[72] J. Tilchin, D. N. Dirin, G. I. Maikov, A. Sashchiuk, M. V Kovalenko, E. Lifshitz, *ACS Nano* **2016**, *10*, 6363.

[73] J. S. Manser, J. A. Christians, P. V. Kamat, *Chem. Rev.* **2016**, *116*, 12956.

[74] W. Wang, Y. Li, X. Wang, Y. Lv, S. Wang, K. Wang, Y. Shi, L. Xiao, Z. Chen, Q. Gong, *Phys. Rev. B* **2016**, *94*, 1.

[75] F. Rossi, *Semicond. Sci. Technol.* **1998**, *13*, 147.

[76] R. Cingolani, L. Calcagnile, G. Col′, R. Rinaldi, M. Lomoscolo, M. DiDio, a. Franciosi, L. Vanzetti, G. C. LaRocca, D. Campi, *J. Opt. Soc. Am. B* **1996**, *13*, 1268.

[77] J. A. Christians, J. S. Manser, P. V. Kamat, *J. Phys. Chem. Lett.* **2015**, *6*, 2086.

[78] Y. Liu, H. Lu, J. Niu, H. Zhang, S. Lou, C. Gao, Y. Zhan, X. Zhang, Q. Jin, L. Zheng, *AIP Adv.* **2018**, *8*, DOI 10.1063/1.5042489.

[79] D. Shi, V. Adinolfi, R. Comin, M. Yuan, E. Alarousu, A. Buin, Y. Chen, S. Hoogland, A. Rothenberger, K. Katsiev, Y. Losovyj, X. Zhang, P. A. Dowben, O. F. Mohammed, E. H. Sargent, O. M. Bakr, *Science.* **2015**, *347*, 519.

[80] M. I. Saidaminov, A. L. Abdelhady, B. Murali, E. Alarousu, V. M. Burlakov, W. Peng, I. Dursun, L. Wang, Y. He, G. Maculan, A. Goriely, T. Wu, O. F. Mohammed, O. M. Bakr, *Nat. Commun.* **2015**, *6*, 7586.

[81] R. Comin, G. Walters, E. S. Thibau, O. Voznyy, Z.-H. Lu, E. H. Sargent, *J. Mater. Chem. C* **2015**, *3*, 8839.

[82] H. Wei, Y. Fang, P. Mulligan, W. Chuirazzi, H.-H. Fang, C. Wang, B. R. Ecker, Y.

Gao, M. A. Loi, L. Cao, J. Huang, *Nat. Photonics* **2016**, *10*, 333.

[83] B. Wu, H. T. Nguyen, Z. Ku, G. Han, D. Giovanni, N. Mathews, H. J. Fan, T. C. Sum, *Adv. Energy Mater.* **2016**, *6*, 1600551.

[84] Z. Zuo, J. Ding, Y. Zhao, S. Du, Y. Li, X. Zhan, H. Cui, *J. Phys. Chem. Lett.* **2017**, *8*, 684.

[85] Y. Fang, Q. Dong, Y. Shao, Y. Yuan, J. Huang, *Nat. Photonics* **2015**, *9*, 679.

[86] B. Murali, S. Dey, A. L. Abdelhady, W. Peng, E. Alarousu, A. R. Kirmani, N. Cho, S. P. Sarmah, M. R. Parida, M. I. Saidaminov, A. A. Zhumekenov, J. Sun, M. S. Alias, E. Yengel, B. S. Ooi, A. Amassian, O. M. Bakr, O. F. Mohammed, *ACS Energy Lett.* **2016**, *1*, 1119.

[87] T. Yamada, Y. Yamada, H. Nishimura, Y. Nakaike, A. Wakamiya, Y. Murata, Y. Kanemitsu, *Adv. Electron. Mater.* **2016**, *2*, 1500290.

[88] T. Yamada, Y. Yamada, Y. Nakaike, A. Wakamiya, Y. Kanemitsu, *Phys. Rev. Appl.* **2017**, *7*, 14001.

[89] S. P. Sarmah, V. M. Burlakov, E. Yengel, B. Murali, E. Alarousu, A. M. El-Zohry, C. Yang, M. S. Alias, A. A. Zhumekenov, M. I. Saidaminov, N. Cho, N. Wehbe, S. Mitra, I. Ajia, S. Dey, A. E. Mansour, M. Abdelsamie, A. Amassian, I. S. Roqan, B. S. Ooi, A. Goriely, O. M. Bakr, O. F. Mohammed, *Nano Lett.* **2017**, *17*, 2021.

[90] X. Chi, K. Leng, B. Wu, D. Shi, Y. Choy, Z. Z. Chen, Z. Z. Chen, X. Yu, P. Yang, Q. Xu, T. C. Sum, A. Rusydi, K. P. Loh, *Adv. Opt. Mater.* **2018**, *6*, DOI 10.1002/adom.201800470.

[91] M. I. Dar, G. Jacopin, S. Meloni, A. Mattoni, N. Arora, A. Boziki, S. M. Zakeeruddin, U. Rothlisberger, M. Grätzel, *Sci. Adv.* **2016**, *2*, e1601156.

[92] J. A. Steele, P. Puech, B. Monserrat, B. Wu, R. X. Yang, T. Kirchartz, H. Yuan, G. Fleury, D. Giovanni, E. Fron, M. Keshavarz, E. Debroye, G. Zhou, T. C. Sum, A. Walsh, J. Hofkens, M. B. J. Roeffaers, *ACS Energy Lett.* **2019**, *4*, 2205.

[93] Y. Kanemitsu, *J. Mater. Chem. C* **2017**, *5*, 3427.

[94] B. Wenger, P. K. Nayak, X. Wen, S. V. Kesava, N. K. Noel, H. J. Snaith, *Nat. Commun.* **2017**, *8*, 590.

[95] B. Bensaid, F. Raymond, M. Leroux, C. Vèrié, B. Fofana, *J. Appl. Phys.* **1989**, *66*, 5542.

[96] L. M. Pazos-Outón, M. Szumilo, R. Lamboll, J. M. Richter, M. Crespo-Quesada, M. Abdi-Jalebi, H. J. Beeson, M. Vrućinić, M. Alsari, H. J. Snaith, B. Ehrler, R. H. Friend, F. Deschler, *Science.* **2016**, *351*, 1430.

[97] R. J. Nelson, R. G. Sobers, *J. Appl. Phys.* **1978**, *49*, 6103.

[98] I. Schnitzer, E. Yablonovitch, C. Caneau, T. J. Gmitter, *Appl. Phys. Lett.* **1993**, *62*, 131.

[99] K.-H. Wang, L.-C. Li, M. Shellaiah, K. Wen Sun, *Sci. Rep.* **2017**, *7*, 13643.

[100] C. A. López, M. V. Martínez-Huerta, M. C. Alvarez-Galván, P. Kayser, P. Gant, A. Castellanos-Gomez, M. T. Fernández-Díaz, F. Fauth, J. A. Alonso, *Inorg. Chem.* **2017**, *56*, 14214.

[101] D. Niesner, M. Wilhelm, I. Levchuk, A. Osvet, S. Shrestha, M. Batentschuk, C. Brabec, T. Fauster, *Phys. Rev. Lett.* **2016**, *117*, 126401.

[102] S. Hu, H. Gao, Y. Qi, Y. Tao, Y. Li, J. R. Reimers, M. Bokdam, C. Franchini, D. Di Sante, A. Stroppa, W. Ren, *J. Phys. Chem. C* **2017**, *121*, 23045.

[103] X. Che, B. Traore, C. Katan, M. Kepenekian, J. Even, *Phys. Chem. Chem. Phys.* **2018**, *20*, 9638.

[104] A. M. A. Leguy, Y. Hu, M. Campoy-Quiles, M. I. Alonso, O. J. Weber, P. Azarhoosh, M. van Schilfgaarde, M. T. Weller, T. Bein, J. Nelson, P. Docampo, P. R. F. Barnes, *Chem. Mater.* **2015**, *27*, 3397.

[105] N. Ahn, D.-Y. Son, I.-H. Jang, S. M. Kang, M. Choi, N.-G. Park, *J. Am. Chem. Soc.* **2015**, *137*, 8696.

[106] X. Tan, B. Zhang, G. Zou, *J. Am. Chem. Soc.* **2017**, *139*, 8772.

[107] J. Yang, B. D. Siempelkamp, D. Liu, T. L. Kelly, *ACS Nano* **2015**, *9*, 1955.

[108] H. He, Q. Yu, H. Li, J. Li, J. Si, Y. Jin, N. Wang, J. Wang, J. He, X. Wang, Y. Zhang, Z. Ye, *Nat. Commun.* **2016**, *7*, 10896.

[109] T. H. Keil, *Phys. Rev.* **1966**, *144*, 582.

[110] A. Sadhanala, F. Deschler, T. H. Thomas, S. E. Dutton, K. C. Goedel, F. C. Hanusch, M. L. Lai, U. Steiner, T. Bein, P. Docampo, D. Cahen, R. H. Friend, *J. Phys. Chem. Lett.* **2014**, *5*, 2501.

[111] E. T. Hoke, D. J. Slotcavage, E. R. Dohner, A. R. Bowring, H. I. Karunadasa, M. D. McGehee, *Chem. Sci.* **2015**, *6*, 613.

[112] S. De Wolf, J. Holovsky, S. J. Moon, P. Löper, B. Niesen, M. Ledinsky, F. J. Haug, J. H. Yum, C. Ballif, *J. Phys. Chem. Lett.* **2014**, *5*, 1035.

[113] M. D. Smith, H. I. Karunadasa, *Acc. Chem. Res.* **2018**, *51*, 619.

[114] E. L. Unger, E. T. Hoke, C. D. Bailie, W. H. Nguyen, A. R. Bowring, T. Heumüller, M. G. Christoforo, M. D. McGehee, *Energy Environ. Sci.* **2014**, *7*, 3690.

[115] B. Murali, E. Yengel, C. Yang, W. Peng, E. Alarousu, O. M. Bakr, O. F. Mohammed, *ACS Energy Lett.* **2017**, *2*, 846.

[116] A. Buin, R. Comin, J. Xu, A. H. Ip, E. H. Sargent, *Chem. Mater.* **2015**, *27*, 4405.

[117] C. M. Sutter-Fella, D. W. Miller, Q. P. Ngo, E. T. Roe, F. M. Toma, I. D. Sharp, M. C. Lonergan, A. Javey, *ACS Energy Lett.* **2017**, *2*, 709.

[118] J. Pospisil, O. Zmeskal, S. Nespurek, J. Krajcovic, M. Weiter, A. Kovalenko, *Sci. Rep.* **2019**, *9*, 1.

[119] S. G. Motti, M. Gandini, A. J. Barker, J. M. Ball, A. R. Srimath Kandada, A. Petrozza, *ACS Energy Lett.* **2016**, *1*, 726.

[120] H. Zhang, Y. Liu, H. Lu, W. Deng, K. Yang, Z. Deng, X. Zhang, S. Yuan, J. Wang, J. Niu, X. Zhang, Q. Jin, H. Feng, Y. Zhan, L. Zheng, *Appl. Phys. Lett.* **2017**, *111*, 103904.

[121] L. M. Falk, K. P. Goetz, V. Lami, Q. An, P. Fassl, J. Herkel, F. Thome, A. D. Taylor, F. Paulus, Y. Vaynzof, *Energy Technol.* **2019**, *1900737*, 1.

[122] C. G. Van De Walle, J. Neugebauer, *J. Appl. Phys.* **2004**, *95*, 3851.

[123] J. Mizusaki, K. Arai, K. Fueki, *Solid State Ionics* **1983**, *11*, 203.

[124] S. Meloni, T. Moehl, W. Tress, M. Franckeviius, M. Saliba, Y. H. Lee, P. Gao, M. K. Nazeeruddin, S. M. Zakeeruddin, U. Rothlisberger, M. Graetzel, *Nat. Commun.* **2016**, *7*, 10334.

[125] M. Sebastian, J. A. Peters, C. C. Stoumpos, J. Im, S. S. Kostina, Z. Liu, M. G. Kanatzidis, A. J. Freeman, B. W. Wessels, *Phys. Rev. B - Condens. Matter Mater. Phys.* **2015**, *92*, 1.

[126] X. Lao, Z. Yang, Z. Su, Z. Wang, H. Ye, M. Wang, X. Yao, S. Xu, *Nanoscale* **2018**, *10*, 9949.

[127] J. Kang, L.-W. Wang, *J. Phys. Chem. Lett.* **2017**, *8*, 489.

[128] W. Zhou, Y. Zhao, X. Zhou, R. Fu, Q. Li, Y. Zhao, K. Liu, D. Yu, Q. Zhao, *J. Phys. Chem. Lett.* **2017**, *8*, 4122.

[129] M. Lai, A. Obliger, D. Lu, C. S. Kley, C. G. Bischak, Q. Kong, T. Lei, L. Dou, N. S. Ginsberg, D. T. Limmer, P. Yang, *Proc. Natl. Acad. Sci. U. S. A.* **2018**, *115*, 11929.

[130] B. Li, L. Fu, S. Li, H. Li, L. Pan, L. Wang, B. Chang, L. Yin, *J. Mater. Chem. A* **2019**, *7*, 20494.

[131] Z.-Y. Zhang, H.-Y. Wang, Y.-X. Y. Zhang, Y.-W. Hao, C. Sun, Y.-X. Y. Zhang, B.-R. Gao, Q.-D. Chen, H.-B. Sun, *Sci. Rep.* **2016**, *6*, 27286.

[132] Y. Yang, Y. Yan, M. Yang, S. Choi, K. Zhu, J. M. Luther, M. C. Beard, *Nat. Commun.* **2015**, *6*, 7961.

[133] Y. Yamada, T. Yamada, A. Shimazaki, A. Wakamiya, Y. Kanemitsu, *J. Phys. Chem. Lett.* **2016**, *7*, 9469.

[134] A. D. Wright, R. L. Milot, G. E. Eperon, H. J. Snaith, M. B. Johnston, L. M. Herz, *Adv.*

*Funct. Mater.* **2017**, *27*, 1700860.

[135] X. Deng, X. Wen, S. Huang, R. Sheng, T. Harada, T. W. Kee, M. Green, A. Ho-Baillie, *J. Phys. Chem. C* **2016**, *120*, 2542.

[136] V. S. Chirvony, S. González-Carrero, I. Suárez, R. E. Galian, M. Sessolo, H. J. Bolink, J. P. Martínez-Pastor, J. Pérez-Prieto, *J. Phys. Chem. C* **2017**, *121*, 13381.

[137] L. Q. Phuong, I. L. Braly, J. K. Katahara, H. W. Hillhouse, Y. Kanemitsu, *Appl. Phys. Express* **2017**, *10*, 1.

[138] T. Handa, D. M. Tex, A. Shimazaki, A. Wakamiya, Y. Kanemitsu, *J. Phys. Chem. Lett.* **2017**, *8*, 954.

[139] B. Dänekamp, N. Droseros, F. Palazon, M. Sessolo, N. Banerji, H. J. Bolink, *ACS Appl. Mater. Interfaces* **2018**, *10*, 36187.

[140] D. Giovanni, H. Ma, J. Chua, M. Grätzel, R. Ramesh, S. Mhaisalkar, N. Mathews, T. C. Sum, *Nano Lett.* **2015**, *15*, 1553.

[141] Z. Guo, J. S. Manser, Y. Wan, P. V Kamat, L. Huang, *Nat. Commun.* **2015**, *6*, 7471.

[142] P. Piatkowski, B. Cohen, F. Javier Ramos, M. Di Nunzio, M. K. Nazeeruddin, M. Grätzel, S. Ahmad, A. Douhal, *Phys. Chem. Chem. Phys.* **2015**, *17*, 14674.

[143] X. Wu, M. T. Trinh, X.-Y. Zhu, *J. Phys. Chem. C* **2015**, *119*, 14714.

[144] T. C. Sum, N. Mathews, *Energy Environ. Sci.* **2014**, *7*, 2518.

[145] O. Malinkiewicz, A. Yella, Y. H. Lee, G. M. Espallargas, M. Graetzel, M. K. Nazeeruddin, H. J. Bolink, *Nat. Photonics* **2013**, *8*, 128.

[146] A. Marchioro, J. Teuscher, D. Friedrich, M. Kunst, R. van de Krol, T. Moehl, M. Grätzel, J.-E. Moser, *Nat. Photonics* **2014**, *8*, 250.

[147] T. Low, V. Perebeinos, R. Kim, M. Freitag, P. Avouris, *Phys. Rev. B* **2012**, *86*, 45413.

[148] H. Wang, J. H. Strait, P. A. George, S. Shivaraman, V. B. Shields, M. Chandrashekhar, J. Hwang, F. Rana, M. G. Spencer, C. S. Ruiz-Vargas, J. Park, *Appl. Phys. Lett.* **2010**, *96*, 81917.

[149] M. B. Price, J. Butkus, T. C. Jellicoe, A. Sadhanala, A. Briane, J. E. Halpert, K. Broch, J. M. Hodgkiss, R. H. Friend, F. Deschler, *Nat. Commun.* **2015**, *6*, 8420.

[150] K. Zheng, K. Žídek, M. Abdellah, J. Chen, P. Chábera, W. Zhang, M. J. Al-Marri, T. Pullerits, *ACS Energy Lett.* **2016**, *1*, 1154.

[151] V. Sharma, S. Aharon, I. Gdor, C. Yang, L. Etgar, S. Ruhman, *J. Mater. Chem. A* **2016**, *4*, 3546.

[152] T. Katayama, H. Suenaga, T. Okuhata, S. Masuo, N. Tamai, *J. Phys. Chem. C* **2018**, *122*, 5209.

[153] A. Mattoni, A. Filippetti, M. I. Saba, P. Delugas, *J. Phys. Chem. C* **2015**, *119*, 17421.

[154] V. Malgras, S. Tominaka, J. W. Ryan, J. Henzie, T. Takei, K. Ohara, Y. Yamauchi, *J. Am. Chem. Soc.* **2016**, *138*, 13874.

[155] T. D. McFarlane, C. S. De Castro, P. J. Holliman, M. L. Davies, *Chem. Commun.* **2019**, *55*, 35.

[156] W. S. Yang, B.-W. Park, E. H. Jung, N. J. Jeon, Y. C. Kim, D. U. Lee, S. S. Shin, J. Seo, E. K. Kim, J. H. Noh, S. Il Seok, *Science.* **2017**, *356*, 1376.

[157] D. W. deQuilettes, K. Frohna, D. Emin, T. Kirchartz, V. Bulovic, D. S. Ginger, S. D. Stranks, *Chem. Rev.* **2019**, *119*, 11007.

[158] V. Sarritzu, N. Sestu, D. Marongiu, X. Chang, Q. Wang, S. Masi, S. Colella, A. Rizzo, A. Gocalinska, E. Pelucchi, M. L. Mercuri, F. Quochi, M. Saba, A. Mura, G. Bongiovanni, *Adv. Opt. Mater.* **2018**, *6*, 1701254.